

University of Windsor

Scholarship at UWindor

Electronic Theses and Dissertations

Theses, Dissertations, and Major Papers

Fall 2021

A Data-Driven Approach using Long-Short Term Memory for Fault Prognosis and Remaining Useful Life Estimation of Satellite Reaction Wheel

Md Sirajul Islam
University of Windsor

Follow this and additional works at: <https://scholar.uwindsor.ca/etd>



Part of the [Mechanical Engineering Commons](#)

Recommended Citation

Islam, Md Sirajul, "A Data-Driven Approach using Long-Short Term Memory for Fault Prognosis and Remaining Useful Life Estimation of Satellite Reaction Wheel" (2021). *Electronic Theses and Dissertations*. 8877.

<https://scholar.uwindsor.ca/etd/8877>

This online database contains the full-text of PhD dissertations and Masters' theses of University of Windsor students from 1954 forward. These documents are made available for personal study and research purposes only, in accordance with the Canadian Copyright Act and the Creative Commons license—CC BY-NC-ND (Attribution, Non-Commercial, No Derivative Works). Under this license, works must always be attributed to the copyright holder (original author), cannot be used for any commercial purposes, and may not be altered. Any other use would require the permission of the copyright holder. Students may inquire about withdrawing their dissertation and/or thesis from this database. For additional inquiries, please contact the repository administrator via email (scholarship@uwindsor.ca) or by telephone at 519-253-3000ext. 3208.

A Data-Driven Approach using Long-Short Term Memory for Fault Prognosis
and Remaining Useful Life Estimation of Satellite Reaction Wheel

By

Md Sirajul Islam

A Thesis
Submitted to the Faculty of Graduate Studies
through the Department of Mechanical, Automotive, and Materials Engineering
in Partial Fulfillment of the Requirements for
the Degree of Master of Applied Science
at the University of Windsor

Windsor, Ontario, Canada

2021

©2021 Md Sirajul Islam

A Data-Driven Approach using Long-Short Term Memory for Fault Prognosis
and Remaining Useful Life Estimation of Satellite Reaction Wheel

By

Md Sirajul Islam

APPROVED BY:

R. Razavi-Far

Department of Electrical and Computer Engineering

A. Cherniaev

Department of Mechanical, Automotive, and Materials Engineering

A. Rahimi, Advisor

Department of Mechanical, Automotive, and Materials Engineering

August 24, 2021

DECLARATION OF CO-AUTHORSHIP/PREVIOUS PUBLICATIONS

I. Co-Authorship

I hereby declare that this thesis incorporates material that is the outcome of my research under the supervision of Dr. Afshin Rahimi who is also the co-author of the papers published through this work. In all cases including the thesis and the papers, the problem definition and the satellite simulator used for generating the raw data come from the previous works done by Dr. Rahimi. The primary contributions/novelty, data analysis, interpretation, and writing were performed by the author and the contribution of the co-author by providing supervision, feedback, and comments.

I am aware of the University of Windsor Senate Policy on Authorship, and I certify that I have properly acknowledged the contribution of other researchers to my thesis and have obtained written permission from each of the co-author(s) to include the above material(s) in my thesis.

II. Previous Publication

This thesis partly includes the original papers that have been previously submitted or published in peer-reviewed journals and conferences, as provided in the following table:

Thesis Chapter	Publication Title/Full Citation	Publication Status
1-6	Sirajul Islam, M.; Rahimi, A. "Fault Prognosis of Satellite Reaction Wheels Using A Two-Step LSTM Network." 2021 IEEE International Conference on Prognostics and Health Management (ICPHM 2021), 1–7, doi:10.1109/ICPHM51084.2021.9486655.	Published
1-6	Sirajul Islam, M.; Rahimi, A. "Use of A Data-Driven Approach for Time Series Prediction in Fault Prognosis of Satellite Reaction Wheel". IEEE International Conference on Systems, Man, and Cybernetics (SMC), 2020, pp. 3624–3628, doi:10.1109/SMC42975.2020.9283435	Published
1-6	Sirajul Islam, M.; Rahimi, A. "A comprehensive data-driven approach for prognosis of a reaction wheel onboard satellite attitude control system.", MDPI Aerospace, [Ref: aerospace-1329421]	Under Review

I certify that I have obtained written permission from the copyright owner(s) to include the above-published material(s) in my thesis. I certify that the above material describes work completed during my registration as a graduate student at the University of Windsor.

III. General

I declare that, to the best of my knowledge, my thesis does not infringe upon anyone's copyright nor violate any proprietary rights and that any ideas, techniques, quotations, or any other material from the work of other people included in my thesis, published or otherwise, are fully acknowledged in accordance with the standard

referencing practices. Furthermore, to the extent that I have included copyrighted material that surpasses the bounds of fair dealing within the meaning of the Canada Copyright Act, I certify that I have obtained a written permission from the copyright owner(s) to include such material(s) in my thesis.

I declare that this is a true copy of my thesis, including any final revisions, as approved by my thesis committee and the Graduate Studies office, and that this thesis has not been submitted for a higher degree to any other University or Institution.

ABSTRACT

Artificial satellites are objects or a body that are stationed in the orbit of another object. The purpose of artificial satellites includes monitoring, information transfer, studying a different planet, space exploration, and fulfilling many other modern-day needs. For the increased demand, the number of artificial satellites revolving around the earth is also increasing. Due to cost efficiency, bulk manufacturing capability, and ease to launch in the orbits, small satellites are the topic of interest. Reaction wheels are widely used in the attitude control system of small satellites. Unfortunately, reaction wheels failure restricts the efficacy of a satellite, and it is one of the many reasons that lead to premature abandonment of the satellites. In larger satellites, there is room for mechanical redundancy to increase service reliability, so an onboard health monitoring system is in demand to ensure seamless performance by minimizing the risk factor of the sudden failure of a small satellite. This study observes the measurable system parameter of a faulty reaction wheel to estimate the remaining useful life of the reaction wheels. In this research, a data-driven approach is for the fault prognosis of the satellite reaction wheel. The measurable system parameters from the satellite reaction wheel are not directly related to the health of the system. So, the proposed method involves three stages to achieve the goal. In the first stage, the necessary observable system parameters are identified, and their future state is predicted based on historical data using a long short-term memory recurrent neural network. A health index parameter is defined and estimated using a multi-variate long short-term memory network in the second stage. In the third stage, the remaining useful life of the reaction wheel is estimated based on historical data of the health index parameter and a threshold. The approach is very efficient depending on the fault severity and can be used in on-field scenarios. The approach is robust up to a certain degree of noise, disturbance, and missing data.

DEDICATION

I am very grateful to get this opportunity to contribute to the field of scientific research, and I would like to dedicate this work to my parents for always believing in me and motivating me to pursue my dream. I am very thankful to my supervisor Dr. Afshin Rahimi for always being available, even in the COVID-19 pandemic, to guide me through my work, and give me mental support. I also want to mention my good friends Abdul Muntakim Rafi, and Hossein Varvani Farahani for encouraging and supporting me when I needed them.

ACKNOWLEDGEMENTS

I have conducted this research work as part of the completion of my Master of Applied Science degree from the University of Windsor. This would not be possible without the support of the Intelligent Control, Analytics, and Modeling (iCAM) lab, and the resources of the University of Windsor. I want to take this opportunity to acknowledge the sincerity and patience of my supervisor Dr. Afshin Rahimi during my early days in the research work as I had very little background in this work. I have learned a lot from him and I express my heartiest gratitude to my supervisor and mentor Dr. A. Rahimi.

I am thankful for all the financial supports that I have received from the University of Windsor and the iCAM lab. Without this financial assistance, it would not be possible for me to complete my study.

I want to thank all the faculty members and staff for making this such a wonderful place to study. I would like to especially thank Dr. Roozbeh Razavi-Far from the Electrical and Computer Engineering Department, and Dr. Aleksandr Cherniaev from the Department of Mechanical, Automotive, and Materials Engineering for taking their valuable time to review my thesis proposal and providing me feedbacks to enrich my research work.

TABLE OF CONTENTS

Declaration of Co-Authorship/Previous Publications	iii
Abstract.....	vi
Dedication	vii
Acknowledgements	viii
List of Tables	xi
List of Figures.....	xii
List of Appendices.....	xiv
List of Abbreviations/Symbols.....	xv
Nomenclature	xvi
1 Chapter 1 Introduction	1
1.1 Introduction	1
1.2 Literature Review.....	2
1.3 Contributions of This Work	5
1.4 Problem Definition.....	5
1.5 Outline.....	10
2 Chapter 2 Theoretical Background	11
2.1 ARIMA.....	11
2.2 LSTM.....	11
2.3 Multivariate LSTM	14
3 Chapter 3 Methodology.....	15
3.1 Data Collection and Preparation	16
3.2 Missing Data Imputation and Noise Addition.....	18
3.3 State Prediction (Stage 1).....	18

3.4	HI Parameter Prediction (Stage 2)	20
3.5	Calculation of RUL (Stage 3).....	24
4	Chapter 4 Case Study: Reaction Wheel onboard satellite.....	25
4.1	Introduction	25
4.2	ACS	25
4.3	Reaction Wheel	26
4.4	Reaction Wheel Assembly	28
4.5	Raw Data Collection and Preparation	29
4.6	Regression models for prognosis	31
5	Chapter 5 Results and Discussion	32
5.1	State Prediction (Stage 1).....	32
5.2	HI Parameter Prediction (Stage 2)	39
5.3	Calculation of RUL (Stage 3).....	40
5.4	Sensitivity Analysis.....	40
6	Chapter 6 Conclusions and Future Works.....	49
6.1	Conclusions	49
6.2	Future Works.....	49
	References	51
	Appendices.....	57
	Appendix A: Copyright Permissions SMC-IEEE.....	57
	Appendix B: Copyright Permissions PHM-IEEE.....	58
	Vita Auctoris.....	59

LIST OF TABLES

Table 1 – ITHACO Type A reaction wheel model system parameters	8
Table 2 – Additional model parameters in MATLAB model for second scale data generation.....	17
Table 3 – Additional model parameters in MATLAB model for day scale data generation.....	17
Table 4 – Additional model parameters in MATLAB model for month scale data generation.....	17
Table 5 – Tuned parameters for the state prediction with the LSTM.....	20
Table 6 – Tuned parameters for kt prediction	22
Table 7 – Impact of training set size on the accuracy of the model.....	36
Table 8 – MSE and NRMS respective to p, d, q values in ARIMA	36
Table 9 – Missing data imputation accuracy for RW speed data	41
Table 10 – Model accuracy for different frequencies in the input dataset.....	42
Table 11 – Model performance degradation for different noise level	45
Table 12 – Tuned parameters and model inputs for kt prediction using day scale dataset	46
Table 13 – Tuned parameters and model inputs for kt prediction using month scale dataset	47

LIST OF FIGURES

Figure 1. Major fault prognosis methods. [9]	2
Figure 2 Different stages of the prognostic model for an RW	6
Figure 3. Bialke’s ITHACO Type A reaction wheel model. [41]	7
Figure 4. LSTM network architecture. Adapted from [46]	11
Figure 5. A chain-like structure of an LSTM network. Adapted from [50], [51]...	12
Figure 6. An LSTM network. Adapted from [11], [37], [43]	13
Figure 7. Structure of multivariate LSTM network. Adapted from [46]	14
Figure 8. Steps toward building the prognostic model for an RW	15
Figure 9. Graph of epoch vs loss for fitting the model to RW speed data	23
Figure 10. Graph of epoch vs loss for fitting the model to motor current data	23
Figure 11. Graph of epoch vs loss for fitting the model to torque command voltage data	24
Figure 12. Graph of epoch vs loss for fitting the model to forecast HI parameter	24
Figure 13. Satellite attitude control system units	25
Figure 14. 16U nanosatellite bus M16P / M16P-R [1]	26
Figure 15. Reaction wheel unit from SSCC lab at Ryerson University. [2]	27
Figure 16. CubeSat Reaction Wheels Control System Sat Bus 4RW0 [57]	28
Figure 17. Raw dataset sample	30
Figure 18. True RW speed data plotted against time	33
Figure 19. Autocorrelation vs lag order of the dataset	34
Figure 20. Adding white gaussian noise to the RW speed dataset	35
Figure 21. RW speed data (test segment) prediction with ARIMA model	35
Figure 22. Fitting reference line for RW speed (ω) prediction	37
Figure 23. Prediction of RW speed data	38
Figure 24. Prediction of motor current data	38
Figure 25. Prediction of torque command voltage data	39
Figure 26. Prediction of HI parameter (kt)	39
Figure 27. Confidence boundary of predicted HI parameter and RUL	40
Figure 28. missing data imputation for 35% ratio of missing.	41

Figure 29. Adding noise to RW speed data	42
Figure 30. Prediction of RW speed data based on noisy dataset	43
Figure 31. Adding noise to motor current.....	43
Figure 32. Prediction on noisy motor current data	44
Figure 33. Adding noise to the torque command voltage.....	44
Figure 34. Prediction of torque command voltage based on noisy data	45
Figure 35. Adding noise to the motor torque coefficient data	45
Figure 36. Prediction of Hi parameter using day scale dataset.....	47
Figure 37. Prediction of HI parameter using month scale dataset	48

LIST OF APPENDICES

Appendix A: Copyright Permissions SMC-IEEE.....	57
Appendix B: Copyright Permissions PHM-IEEE.....	58

LIST OF ABBREVIATIONS/SYMBOLS

RW	Reaction Wheel
ACS	Attitude Control System
LSTM	Long Short-Term Memory
WPT	Wavelet Packet Transform
ANN	Artificial Neural Networks
FDI	Fault Detection and Isolation
CBM	Condition Based Monitoring
PHM	Prognostic Health Monitoring
FFT	Fast- Fourier Transform
AR	Auto Regressive
ARMA	Auto Regressive Moving Average
ARIMA	Auto Regressive Integrated Moving Average
RNN	Recurrent Neural Network
RUL	Remaining useful life
UKF	Unscented Kalman filter
SVM	Support vector machine
HI	Health Index
NRMS	Normalized root mean squared error
RMS	Root mean squared error
FSS	Fine Sun Sensor
CSS	Coarse Sun Sensor
SPS	Sun Present & Sun not Present
ES	Earth Sensor
MGM	Magnetometers
GYR	Gyroscope
STR	Star Sensor
GPS	Global Positioning System
RW	Reaction Wheel
MW	Momentum Wheel
MGT	Magnetorquers
CMG	Control Moment Gyros

NOMENCLATURE

ω	Reaction wheel angular speed
I_m	Motor current
V_{comm}	Torque command voltage
V_{bus}	Bus voltage
k_t	Motor torque
ω_m	Motor angular speed
G_d	Driver gain
T	Temperature
I_{bus}	Bus current
K_e	Back electromotive force voltage gain
f_1	Motor disturbance term
f_2	Motor disturbance term
f_3	The electromotive torque limiting block
f_4	Approximation of the sign function in the coulomb friction block
f_5	Speed limiter block
F_p	Fault parameter matrix
f_p	Fault parameter
B	Ripple torque
C	Cogging torque
R_B	Bridge resistance
K_f	Voltage feedback gain
K_s	Over-speed circuit gain
N	Window size
N_s	Number of samples
μ	Gravitational constant parameter
\mathcal{T}_{noise}	Torque noise disturbance
\mathcal{T}_V	Viscous torque
ω_d	Driver bandwidth
ω_s	Maximum wheel speed
\mathcal{T}_d	Other disturbance
\mathcal{T}_c	Control torque applied by the momentum exchange device
R_{IN}	Input filter resistance
t	Time

CHAPTER 1

INTRODUCTION

1.1 Introduction

In modern days, small satellites are our subject of interest for their low manufacturing cost, ease to launch into orbit, and the capability to deliver the same outcome as their large counterparts. Reaction wheels (RW)s are an integral part of the attitude control system (ACS) of a small satellite to have control over the rotation of its axes. To perform the designated task, a satellite needs to have accurate control over its direction. Though the RWs are very efficient, they are very prone to failure, and for a small satellite, that can lead to a disaster resulting in complete failure of the satellite. As there is not much room for mechanical redundancy in a small satellite to enhance the reliability and useful lifetime, one needs to increase the analytical redundancy as an alternative solution. If we monitor the degradation of performance in the attitude control system properly and estimate the remaining useful life (RUL) of the system, we can avoid a potential disaster and downtime of the service. Often, the cause of mechanical failure in RW is inadequate bearing lubrication and uneven frictional torque. This fault can be monitored from motor torque variation. In this study, we develop a data-driven fault prognosis model to predict the RUL of a faulty RW onboard satellite.

Many studies are found in the field of condition-based monitoring (CBM) and prognostics health monitoring (PHM). However, only a few are dedicated to satellite reaction wheels. Studies show a 200% growth in microsatellites launches in the last five years [1]. It draws attention to develop a data-driven approach that can take the measurable sensor data as input and return the expected remaining useful life of the system under incipient fault. Developing a model-based prognostic method for a complicated system is very difficult as it requires a lot of system information. The prognosis of satellite RWs is a modern-day problem and there are a few model-based studies [2]–[8] found that address this topic with limited success. So, data-driven techniques are getting popular for less dependency on the system information.

1.2 Literature Review

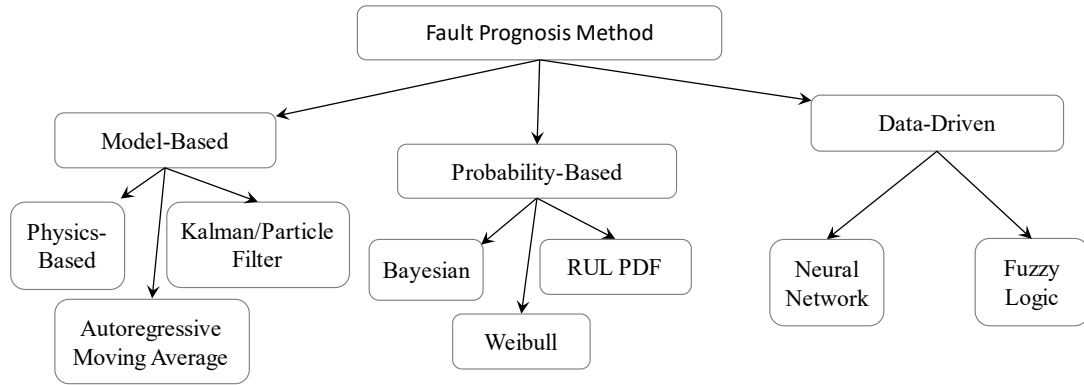


Figure 1. Major fault prognosis methods. [9]

Many data-driven studies are found in the field of prognosis, but only a handful of them ([2], [10]–[12]) are directly related to the fault prognosis of RW in ACS onboard satellites. The authors in [3] have proposed a model-based approach to predict the RUL of an RW onboard satellite. The authors claim the model performs considerably well in the prediction of RUL with the error ranging from 1.5 to 13 percent, but the prediction interval shows the uncertainty in prediction increases with time.

The authors in [13] have developed a two-step data-driven approach using the Kolmogorov-Smirnov test, self-organize map, and an unscented Kalman filter (UKF) for bearing fault prognosis. In step one, the authors model the degradation process by learning the degradation. In the second step, degradation data and UKF is combined to predict the RUL. However, the method requires a significant amount of training data to perform meaningfully. In [14], the authors developed and implemented a multi-scale extended Kalman filter (EKF) using real motor data from an RW in satellite to predict RUL. In the process, the motor’s dynamic behaviour is expressed by an ordinary differential equation, and the authors use the damping co-efficient as a health indicator.

Some statistical model-based and data-driven approaches for machine fault diagnosis and prognosis are discussed in [15]. The authors in [16] defined and combined three goodness metrics of correlation, monotonicity, and robustness of the rolling element for degradation

feature selection during the RUL prediction. In [17], the authors have used wavelet packet transform and an artificial neural network for rolling element RUL prediction. Both proposed methods can be used for any similar system, and the outcome and robustness can be improved if the model can be trained with data from multiple systems.

In [18], the authors have used experimental data and suggested a condition monitoring technique for bearing life enhancement and preventing torque inequality by controlling the lubrication process. The authors propose a method using support vector machine (SVM) regression in [19] for wear assessment of cutting tools and calculation of RUL. The proposed method is based on feature extraction, and it requires adequate training data for the model to predict meaningfully. The method uses a combined feature found by dimensionality reduction and uses it as a health index (HI) parameter. In the end, the HI parameter is mapped to a non-linear regressor for RUL prediction.

In [20], variational mode decomposition (VMD) and long short-term memory (LSTM) recurrent neural networks (RNN) are used for the prediction of rotary machinery health. The authors in [21] have used a Feedforward artificial neural network (ANN) with a Marquardt training algorithm to predict the RUL of a bearing. The proposed ANN model uses time, and measurements of Weibull Hazard rates of root mean squared (RMS) and kurtosis from its present and previous points as input and returns normalized life percentage as output.

The authors in [22]–[26] have studied and implemented different available techniques for the prognosis of rotary machinery. Different stages of CBM and PHM are mentioned in these articles, such as data collection, feature selection, state prediction using ANN. The authors have summarized several contemporary works in prognosis till the date of publication of their research.

In [27], the authors mentioned an intelligent technique for the CBM and PHM of the common rotary component in a system. In this process, vibrational data from the sensor is used as an input, and feature extraction is carried out using a sparse auto-encoder. The authors used a moving average filter before feeding the data to the model. The model returns an auto-encoder correlation-based rate (AEC) as output, and AEC is used to understand the condition of the rotary machinery. A method for CBM of rotary machinery using vibration data and the sound of working conditions is also mentioned in [28].

In [29], the authors used the Fourier transform and an auto-encoder to identify high-level features for PHM of rotary machinery. The model predicts the RUL with reasonably good accuracy, but the model performance degrades with noise. The model can be used in a similar scenario of PHM in any system, where vibration analysis is used. In [30], the authors have studied acoustic emission, vibration data, acoustic technique, the shock pulse method, thermal and wear debris monitoring for CBM of mechanical and electrical devices. The authors in [31] have proposed a multidimensional technique using SVM and particle filter-based method for PHM of rotary machinery. The mentioned approach is claimed to be better in estimating RUL than the methods using data from single sensors. On the contrary, the model complexity in [31] is higher, making it unsuitable for complex systems that require a faster response.

Some statistical model-based and data-driven approaches for CBM and PHM are briefly discussed in [32]. The authors in [33]–[35] have used the COVID-19 data set of infected people to predict the peak during the wave of infection and estimated time to reach that state. The authors have used different state-of-the-art machine learning techniques for the regression analysis in these papers.

LSTM is an effective RNN for regression analysis and feature selection. The fundamentals and different applications of the LSTM model are discussed in [20], [36]–[40]. The authors of [11] have proposed a two-step prognosis technique for satellite RW and carried out a state parameter prediction. The authors used an auto-regressive integrated moving average (ARIMA) model, and an LSTM network for state parameter prediction and the best accuracy obtained by each model has a normalized root mean squared error (NRMS) 0.138 and 0.04, respectively.

In this study, a novel comprehensive three-step data-driven approach for the prognosis of the satellite reaction wheel is proposed to address the limitation in literature as discussed above. In the first step, state parameter prediction is carried out. In the second step, the health index parameter is defined and predicted. Finally, in the third step, with the help of historical data and a threshold, the RUL of an RW in the attitude control system onboard satellite is estimated.

1.3 Contributions of This Work

Contributions of this work are listed and described below:

[CONTRIBUTION 1] Developing a new three-stage data-driven prognostic technique using long-short term memory (LSTM) recurrent neural network (RNN). The accuracy achieved in prediction of health index (HI) parameter is normalized root mean squared (NRMS) error (0.01~0.02), and the accuracy in prediction of remaining useful life (RUL) is 1% ~ 2.5%.

1.4 Problem Definition

Reaction wheels were first introduced in automobiles to conserve momentum and provide smooth power output. The same idea can be used for many purposes. In a satellite attitude control system, the reaction wheels are used for a different purpose. Particularly in small satellites, RWs are used to rotate the satellite on its axis. It is done using an electric motor to rotate the RW to obtain an equal and opposite momentum to rotate the satellite in the opposite direction. Multiple RWs can be assembled in different configurations to gain 3-axis attitude control. As a result, the method became very popular for cost-efficient satellite manufacturing and service. However, the reaction wheel as a mechanical device does not have a long lifespan, and in the case of small satellites, there is not much room for mechanical redundancy to improve reliability. Furthermore, installing an increased number of RWs in satellites increases the weight and launch cost, which contradicts the key financial aspect of small satellites. To overcome this problem, proper CBM and PHM techniques can be used to increase service reliability as they will nullify the service downtime due to RW failure by providing an estimated RUL of the system.

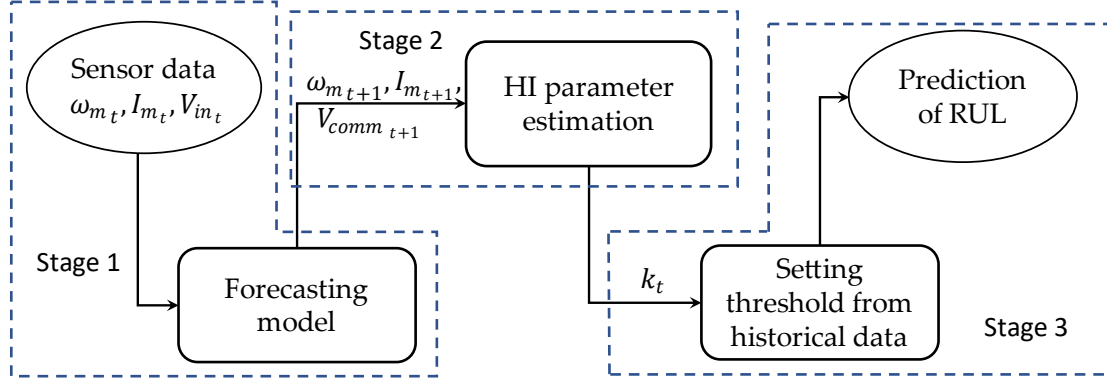


Figure 2 Different stages of the prognostic model for an RW

This study aims to predict the remaining useful life of a reaction wheel under incipient fault using a data-driven approach. To achieve this goal, a three-step process is proposed. Figure 1 illustrates the flow of the proposed three-step process followed during the prognosis of RW in this study. The main components of RW that are prone to failure are bearing and electrical motor. The developing fault can be monitored by motor torque (k_t) and bus voltage (V_{bus}). Neither of the bus voltage or motor torque data is available from the sensor readings. The available essential sensor readings are wheel speed (ω_m), motor current (I_m), and torque command voltage V_{comm} .

The mathematical relation between system states motor current I_m , RW speed ω_m and HI parameter motor torque coefficient (k_t) is expressed in Equation (1), and the relationship is highly nonlinear. Figure 3 represents Bialke's ITHACO type A reaction wheel. The system parameters and constants for the ITHACO Type-A reaction wheel by Goodrich modelled by Bialke are listed in Table 1. Due to the nonlinearity in the mathematical relation, numerical simulations are used to generate accurate input data. A detailed description of Bialke's high fidelity reaction wheel model can be found in [41].

The nonlinear RW model can be mathematically expressed as follows [42]:

$$\begin{aligned}
 \dot{I}_m &= G_d \omega_d [f_3(\omega_m, I_m) - f_5(\omega_m)] - \omega_d I_m + G_d \omega_d V_{comm} \\
 \dot{\omega}_m &= \frac{1}{J_w} \{f_1(\omega_m) + k_t I_m [f_2(\omega_m) + 1] - \tau_v \omega_m - \tau_c f_4(\omega_m) + \tau_{noise}\}
 \end{aligned} \tag{1}$$

In which,

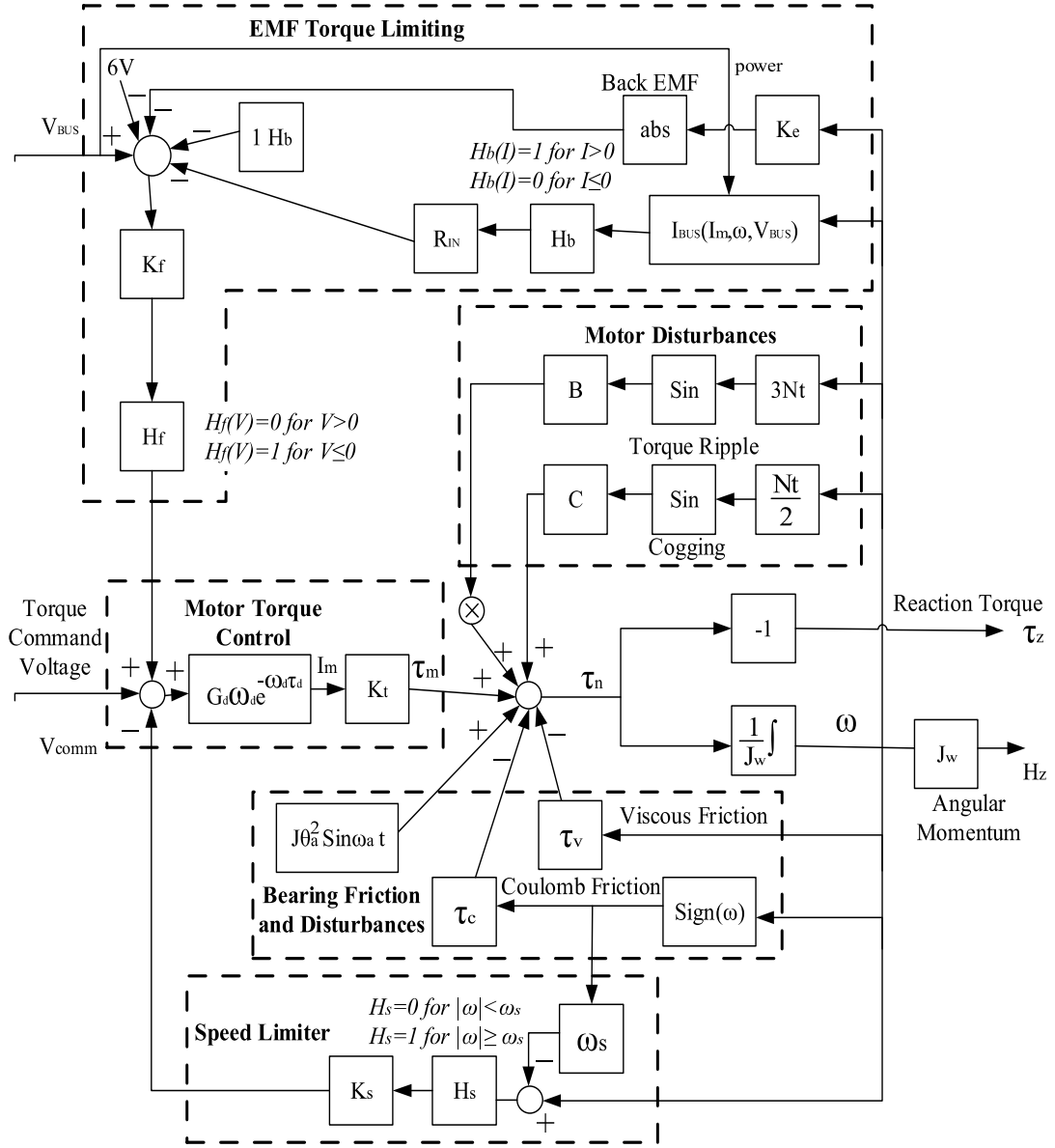


Figure 3. Bialke's ITHACO Type A reaction wheel model. [41]

$$f_1(\omega) = C \sin\left(\frac{Nt}{2} \omega_m\right)$$

$$f_2(\omega) = B \sin(3Nt \omega_m)$$

$$f_3(\omega_m, I_m, V_{bus}) = \frac{\exp[-aV(\omega_m, I_m, V_{bus})]}{1 + \exp[-aV(\omega_m, I_m, V_{bus})]} V(\omega_m, I_m, V_{bus})$$
(2)

$$f_4(\omega) = \frac{1 - \exp(-a\omega)}{1 + \exp(-a\omega)}$$

$$f_5(\omega) = \frac{k_s[\omega_m - \omega_s f_4(\omega)]}{2} \left\{ \frac{1}{1 + \exp[-a(\omega_m - \omega_s)]} + \frac{1}{1 + \exp[a(\omega_m + \omega_s)]} \right\}$$

$$V(\omega_m, I_m, V_{bus})$$

$$= k_f \left[V_{bus} - 6 - \frac{1}{1 + \exp(-aI_{bus})} (1 + R_{in} I_{bus}) - \frac{1 - \exp(-ak_e \omega_m)}{1 + \exp(-ak_e \omega_m)} k_e \omega_m \right]$$

Table 1 – ITHACO Type A reaction wheel model system parameters

Parameter	Value
Coulomb Friction (τ_c)	0.002 Nm
Viscous Friction (τ_v)	3.84×10^{-4} Nm/rad/s
Drive gain time constant (τ_d)	0.245
Ripple Torque (B)	0.22
Temperature (T)	23° C
Cogging Torque (C)	0
Torque Noise Frequency (ω_a)	0.2 rad/sec
Jitter Angle (θ_a)	0.05 rad = 3 degrees
BEMF (K_e) Nominal	0.029 V/rad/s
Motor Torque Const. (k_t)	0.029 Nm/A
Bus Voltage (V_{bus}) Nominal	8 V
Bridge Resistance (R_B)	2 Ω
Driver Gain (G_d)	0.19 A/V
Number of Motor Poles (N)	36
Input Filter Resistance (R_{IN})	2 Ω
Quiescent Bus Power (P_q)	3 W
Driver Bandwidth (ω_d)	9 rad/s
Voltage Feedback Gain (k_f)	0.5 V/V
Over-speed Circuit Gain (k_s)	95
Maximum Wheel Speed (ω_s)	680 rad/s

There are five building blocks (f_{1-5}) inside Bialke;'s RW model. Where, f_1 and f_2 capture the motor disturbance, f_3 accounts for EMF torque-limiting block, f_4 addresses analytical approximation of the sign function, and f_5 stands for the speed limiter block. A detailed explanation of these blocks and Equation (1), & (2) can be found in [42].

The goal of this research is to develop a comprehensive data-driven model for the prognosis of satellite RW. The relation between the states and the HI parameter is highly nonlinear [42]. Therefore, in the first stage of this work, forecasting the future data (RW speed ($\omega_{m_{t+1}}$), motor current ($I_{m_{t+1}}$), torque command voltage ($V_{comm_{t+1}}$)) using a forecasting model and the available measurements (RW speed (ω_{m_t}), motor current (I_{m_t}), torque command voltage (V_{comm_t})). In the second stage of the proposed approach, the HI parameter is defined to be k_t and employed a degradation model to find forecasted states for this parameter using the degradation model and historical and available measurements from the system. Finally, in the third stage of the proposed approach, a threshold for the HI parameter (k_t) is established from the historical data and compared with the data found in the second stage to predict the RUL

Based on previous studies by [7], [43], [44] on electrical motors degradation behaviour for a similar system, the degradation of system health is related to k_t is considered to be exponential growth or decline. This can be mathematically modeled as [45]

$$k_t = ae^{-bt} \quad (3)$$

Wherein, a and b are the model parameter to be estimated and t is the respective time. A detailed explanation of the degradation model for k_t can be found in [2]. This logic is used for developing an RW model with induced incipient fault for data acquisition to use in this research for developing a data-driven fault prognosis method for an RW.

Limitation and assumptions made in this research are as follows:

- During this research and analysis simulator generated data is used.
- The prognostic model is developed based on Bialke's high fidelity RW model.
- The threshold for health index parameter is selected at 30 percent of the nominal value as in [2]

1.5 Outline

The rest of this document is structured as follows:

In chapter 2, the theoretical background for satellite RW fault prognosis is presented. The detailed methodology to solve this problem is in chapter 3. Next, in chapter 4, a case study is presented with the implementation of the proposed methodology for the evaluation of the model. Then, in section 5, results are presented and discussed. Finally, in chapter 6, a conclusion and remarks for future works and applications are provided.

CHAPTER 2

THEORETICAL BACKGROUND

In this chapter, some theoretical backgrounds are provided that are necessary to support the proposed scheme for this thesis.

2.1 ARIMA

ARIMA is a mathematical model specially designed for regression of complex and non-stationary time series. The ARIMA model can be mathematically written as

$$\dot{y}_t = c + \phi_1 \dot{y}_{t-1} + \dots + \phi_p \dot{y}_{t-p} + \theta_1 \varepsilon_{t-1} + \theta_q \varepsilon_{t-q} + \varepsilon_t \quad (4)$$

where \dot{y}_t is the series after differentiating y_t , and it can be done more than multiple times. The prediction contains both the lagged values of y_t and lagged error. The model is known as ARIMA (p, d, q) model. The relationship between p, d, and q can be expressed as

$$(1 - \phi_1 B - \dots - \phi_p B^p)(1 - B)^d y_t = c + (1 + \theta_1 B + \dots + \theta_q B^q) \varepsilon_t \quad (5)$$

where $(1 - \phi_1 B - \dots - \phi_p B^p)$, $(1 - B)^d y_t$ and $c + (1 + \theta_1 B + \dots + \theta_q B^q) \varepsilon_t$ are expressed as p, d, q, respectively. p is the order of the autoregressive part (lag order), d is the degree of first differencing involved and, q is the order of the moving average

2.2 LSTM

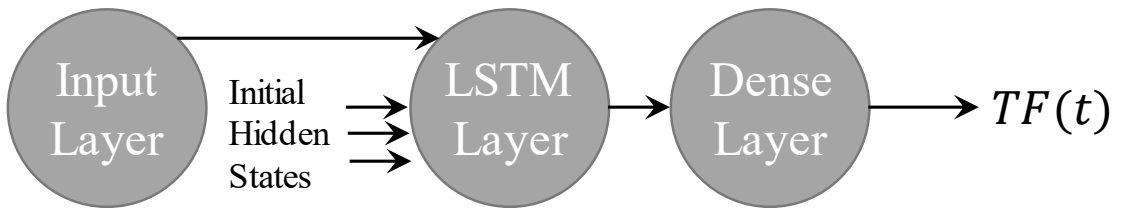


Figure 4. LSTM network architecture. Adapted from [46]

LSTM is a specially designed RNN that can address long term dependency issue that exists with conventional RNN. LSTM was first proposed by Hochreiter and Schmidhuber [36]. Currently, there are many versions of the LSTM network available. However, the LSTM network used in this study is adapted from [47]–[50]. LSTM has a chain-like structure similar to all other standard RNNs; however, the repeating module in LSTM has a different

structure with interactive layers. The components of each block inside an LSTM network are shown in Figure 5.

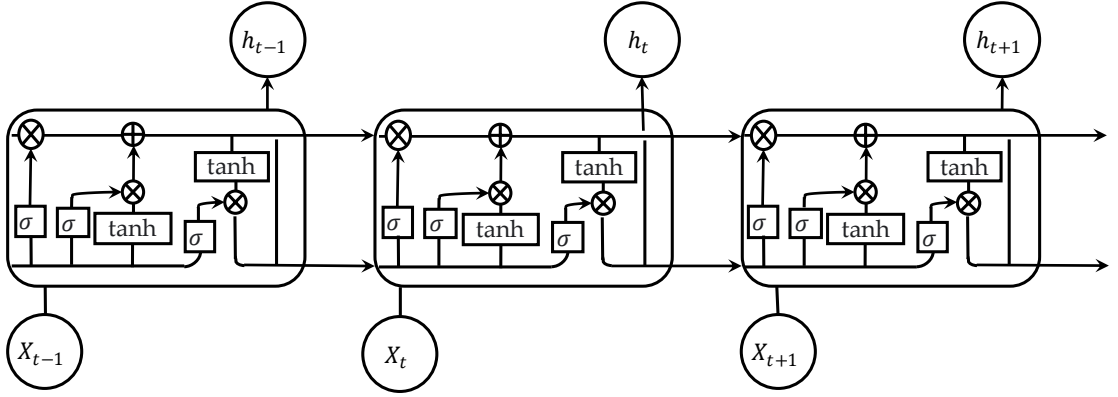


Figure 5. A chain-like structure of an LSTM network. Adapted from [50], [51]

LSTM networks work with memory blocks instead of neurons where the memory blocks are connected through layers. Each block in Figure 5 takes a sequence of input, and a sigmoid function determines the activation of gates inside the block. Equation (6) represents a sigmoid activation function. The first step inside an LSTM network block is a forget gate to decide which information to dispose of from the cell state. Equation (7) mathematically represents a forget gate. The next step has two parts. The input gate layer decides which values will be updated in the first part, as shown in Equation (8). In the second part, a $\tanh(\cdot)$ layer creates new values to add to the state in Equation (9). Later, these two parts are multiplied to update the state in Equation (10). Finally, the block decides the output in the output gate step. In this step, at first, a sigmoid function decides which part of the cell state to pass as output, using Equation (11). Subsequently, the cell state from the input gate passes through $\tanh(\cdot)$ and is multiplied with the output of the output gate, using Equation (12). As a result, the output gate inside the LSTM block can provide the final output for the block.

$$\sigma(t) = \frac{1}{1+e^{-t}} \quad (6)$$

$$f_t = \sigma(W_f \cdot [h_{t-1}, x_t] + b_f) \quad (7)$$

$$i_t = \sigma(W_i \cdot [h_{t-1}, x_t] + b_i) \quad (8)$$

$$\tilde{C}_t = \tanh(W_C \cdot [h_{t-1}, x_t] + b_C) \quad (9)$$

$$C_t = f_t \times C_{t-1} + i_t \times \tilde{C}_t \quad (10)$$

$$o_t = \sigma(W_o[h_{t-1}, x_t] + b_o) \quad (11)$$

$$h_t = o_t \times \tanh(C_t) \quad (12)$$

In Equations (6)-(12), W_f , W_i , W_C , and W_o are the weights of the forget gate, input gate, $\tanh(\cdot)$, and output gate, respectively, h_{t-1} is the output from previous block, x_t is current time steps contribution, C_{t-1} is the contribution of $\tanh(\cdot)$ from previous block at time step (t-1), and terms b_f , b_i , b_C , and b_o are the biases.

LSTM network is a kind of recurrent neural network that overcomes the vanishing gradient problem. So, it can be used when working with difficult sequence problems in machine learning. LSTM network can overcome long-term dependency problems in RNN. Figure 6 shows an illustrated view of a block inside an LSTM network.

In LSTM, blocks are used instead of neurons, and the blocks are more effective than neurons as the blocks can select whether to update the information depending on the conditions. A block comprises three gates; a forget gate, an input gate, and an output gate, which manage the state and output of the block.

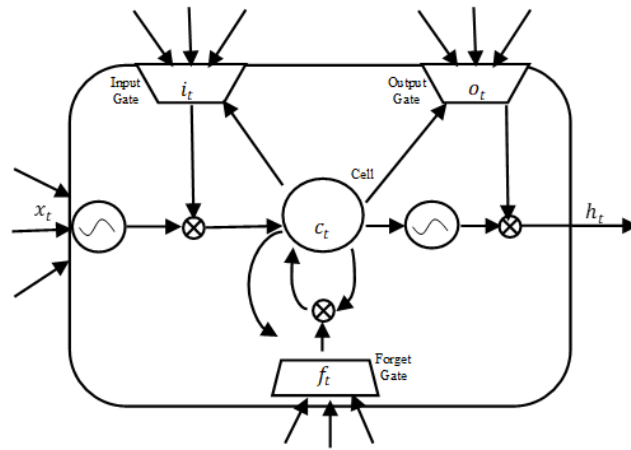


Figure 6. An LSTM network. Adapted from [11], [37], [43]

2.3 Multivariate LSTM

A multivariate LSTM network is an LSTM network that works with the principle of many to one. This network is capable of taking several different kinds of inputs and providing a single output. This network is very efficient in the prediction of complicated time series where the output of the network is dependent on multiple other conditions inherently. Figure 7 shows the structure of a multivariate LSTM network where the network is adapted to take three different features as input and provide a single output.

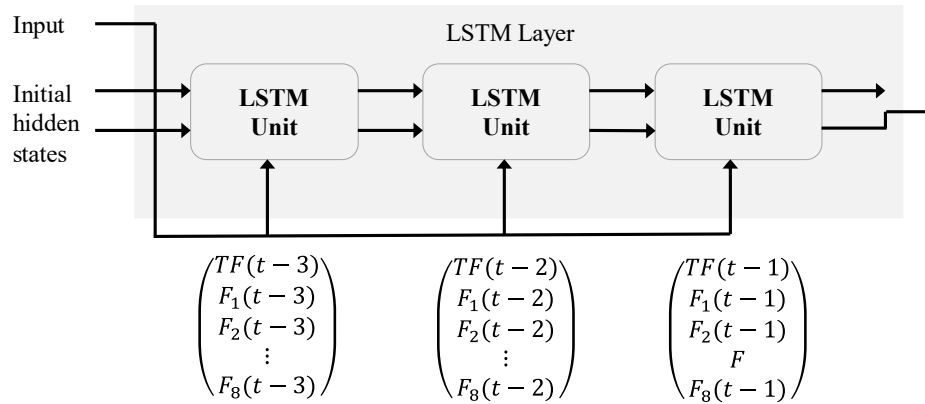


Figure 7. Structure of multivariate LSTM network. Adapted from [46]

CHAPTER 3

METHODOLOGY

For the data-driven fault prognosis of satellite RW, an optimized machine learning method is developed to forecast the time-series dataset. Figure 8 shows the steps followed during the selection of the final model for time series prediction and the steps followed towards building the prognostic model for an RW. The models used during this process are autoregressive (AR), autoregressive moving average (ARMA), autoregressive integrated moving average (ARIMA), and recurrent neural network long-short term memory (LSTM), multi-variate LSTM. In Figure 8, the flowchart shows the main steps towards building the prognostics model for a satellite RW.

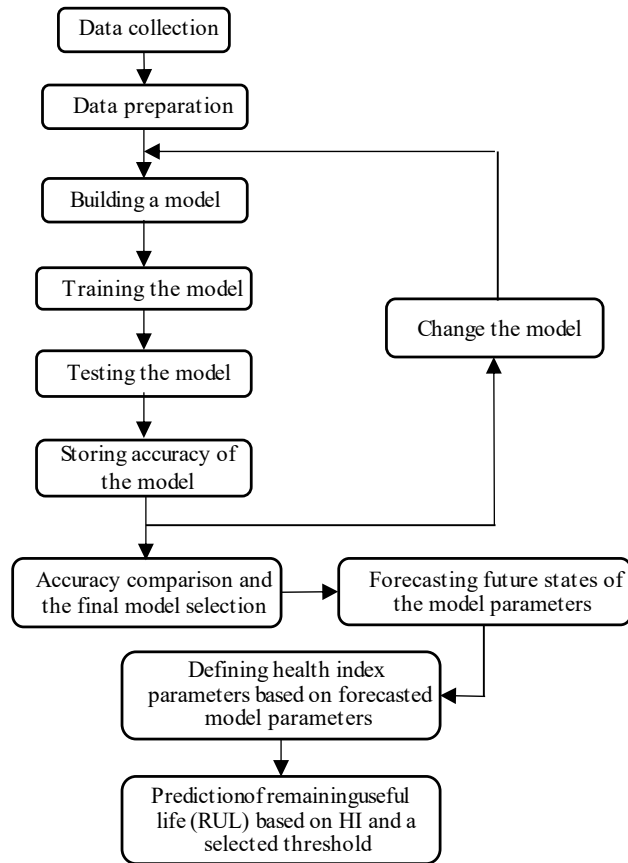


Figure 8. Steps toward building the prognostic model for an RW

Figure 8 shows the reasonable structure blocks followed during this study to build the model for predicting the reaction wheel system states in a satellite attitude control system. The principal methodology is to choose a reasonable regression model for predicting the future trend and behaviour of the available system states. In this study, LSTM is selected to provide very accurate regression results for the reaction wheel speed dataset [11]. One regression model can perform superior to another depending on the dataset type and adjustment of model parameters.

3.1 Data Collection and Preparation

Generally, for data-driven prognosis approaches, the raw data to train and test a model is collected from the functioning hardware or a computer simulation from a digital twin of the hardware. The real-life data from a satellite attitude control system is not easily accessible, making the data-driven fault prognosis more difficult. This is overcome by producing synthetic data from a computer-generated model. Bialke's ITHACO Type-A high fidelity model is used, as shown in Figure 2 and formulated in Equation (1), to generate synthetic data and further add Gaussian white noise to the dataset to resemble the dataset from a real-life satellite.

For the simulation, all the variables and the assumptions are set as stated in Table 1 and inserted an incipient fault in the k_t the module of the model. The model is run for 15000 seconds and stored the model output taking time step 0.1 seconds. This generates 150000 data points for each output of the model. The model outputs are, RW speed (ω), motor current (I_m), Torque command voltage (V_{comm}), motor torque coefficient (k_t), and bus voltage (V_{bus}). Where ω , I_m , and V_{comm} are the measurements that are available from sensor reading in case of an operational satellite and k_t , V_{bus} are non-measurable system parameters that we can use for RW health monitoring. The data is stored in a CSV file format for analyzing and building a data-driven fault prognosis model. Further added Gaussian white noise to the dataset to resemble the dataset from a real-life satellite. The additional model parameters and functions that are changed during inserting incipient fault and generating data is stored in Table 2, Table 3, and Table 4. The analysis using second scale data is shown in result section and sensitivity analysis and the analysis using the day and month scale data is added in the sensitivity analysis section.

Table 2 – Additional model parameters in MATLAB model for second scale data generation

Parameter/ function name	Parameter value / function
Data sampling rate	0.1 per second
Frequency input	0.1Hz
Simulation duration	15000s
k_t incipient fault	$k_t = k_{t_0}(1/\exp(t*1e - 4))$

Table 3 – Additional model parameters in MATLAB model for day scale data generation

Parameter/ function name	Parameter value / function
Data sampling rate	1 per second
Frequency input	0.01Hz
Simulation duration	1400000s
k_t incipient fault	$k_t = k_{t_0}(1/\exp(t*1e - 6))$

Table 4 – Additional model parameters in MATLAB model for month scale data generation

Parameter/ function name	Parameter value / function
Data sampling rate	2 per second
Frequency input	0.01Hz
Simulation duration	13200000s
k_t incipient fault	$k_t = k_{t_0}(1/\exp(t*1e - 7))$

3.2 Missing Data Imputation and Noise Addition

In this study, model-generated data is used, making our dataset free from impurity. However, there can be missing values, additional disturbance, or noise in the data from real-life sources due to errors in the sensor reading or other uncertainties. To ensure real-life implications, it is crucial to address these issues. Randomly erased data using the Python function and added Gaussian white noise to the dataset to emulate the real-world scenario. The per cell probability of missing value can be expressed by Equation (16). Where, $P(X \in S)$ represents probability of X taking a value in a set, Ω is sample space, and ω is out come of the sample space [52]. When working with missing data, interpolation techniques are used to impute the missing values. In Equation (13), the interpolation function for missing value imputation can be found, and Equation (14) defines a white Gaussian. Where, $S_X(f)$ flat power spectral density, μ_X is mean, and $\frac{N_0}{2}$ is a constant. LSTM network can also address the missing data issue but in this case a simple interpolation technique has proven to be effective enough. We calculate and express the noise quantity signal to noise ratio (SNR) in decibel unit quantity during the research. The function used for the calculation of noise level can be found in Equation (15).

$$y = y_1 + (x - x_1) \frac{(y_2 - y_1)}{(x_2 - x_1)} \quad (13)$$

$$S_X(f) = \frac{N_0}{2}, \text{ for all } f, \quad \mu_X = 0 \quad (14)$$

$$SNR = 20 \log \frac{S}{N} \quad (15)$$

$$P(X \in S) = P(\{\omega \in \Omega \mid X(\omega) \in S\}) \quad (16)$$

3.3 State Prediction (Stage 1)

In this study, available measurements are the RW angular speed (ω), Motor current (I_m), and torque command voltage (V_{comm}). An LSTM network is used for the prediction of future measurements. The utilized LSTM network incorporates a visible input layer, a hidden layer comprising four LSTM blocks, and an output layer. A customized Adam optimizer is used for learning rate and faster convergence. The Adam optimizer is customized

using a scheduler with a learning rate decay rate of 0.85 for every 10 epochs. A large initial learning rate helps the network learn faster and reduce computational time, but it can conclude to a suboptimal solution [53]. Hence, the use of a scheduler solves the problem for the network to learn faster and efficiently. The model is trained with 70 percent of the dataset and tested with the remaining of the dataset. For validation, 25 percent of the dataset is used. The predicted measurements are stored and used for state or HI parameter prediction. However, when predicting the data after the available dataset, we need to predict based on the prediction in the previous time step. This causes even a minor error in the prediction of the first-time step to propagate through the next prediction. We assist our model to overcome this problem by using a reference line. The reference line is formed as

$$y(t) = A_1 \times e^{(\log(b_1) \times t)} + (A_2 \times e^{(\log(b_2) \times t)}) \times \sin(f_{max} \times \omega \times t + p) + c \quad (17)$$

where, A_1 , b_1 , A_2 , b_2 , ω , p , c are all unknown constants, t denotes time, and f_{max} is maximum frequency obtained from a fast Fourier transform (FFT) of the dataset. All unknown constants in Equation (17) are found using a nonlinear least-square fit of the dataset to Equation (17). This equation is developed after analysing the true data pattern where, the true data has different frequencies in it and by Fast Fourier Analysis the frequencies are separated. The data pattern also show an exponential decline pattern and that is address by the first part of the equation (17).

3.3.1 *Adjusting Hyperparameters*

For any neural network, it is imperative to adjust and the model's hyperparameter according to the dataset. All the tuned parameters for the state prediction with the LSTM network are listed in Table 5,

Table 5 – Tuned parameters for the state prediction with the LSTM

Parameter	Value
Train to total data ratio	70%
Optimizer	ADAM
Initial learning (LR) rate	0.002
LR decrement per 10 epochs	85%
Validation split	25%
Batch size	128
Degree of differencing (L_B)	16
Number of epochs	1000
Number of future data Prediction	100,000
Number of total data points in each feature	150,000
Data normalization	0-1
Data sampling rate	0.1second

3.3.2 Loss function

For the proposed LSTM network mean squared error (MSE) loss function is used. This is the most commonly used loss function in neural networks. MSE loss function is very effective during the regression analysis with the neural. As the name states in this loss, function loss are calculated by taking the mean squared difference between the predicted value and true data. Mathematically it can be expressed as follows:

$$L(y, \hat{y}) = \frac{1}{N} \sum_{i=0}^N (y - \hat{y}_i)^2 \quad (18)$$

wherein, \hat{y} is the predicted value and y is true data.

3.4 HI Parameter Prediction (Stage 2)

The main goal for our study is to predict the remaining useful life of the reaction wheel, so we determine the HI parameter in this stage from measurable sensor data. A multi-variate LSTM network is used for the calculation of HI parameter motor torque coefficient (k_t).

We take wheel speed (ω_m), motor current (I_m), and torque command voltage (V_{comm}) as inputs to train the model, and we calculate loss during training from the available motor torque data from the model. During training, 70 percent of the total data is used, and the rest are used to test the model performance. For validation, 30 percent of the dataset is used. A custom Adam optimizer with a decremental learning rate is used for efficient training.

As there are different types of frequencies in the input data, we use two types of filters in the input data before feeding them to the model to assist model performance. For RW speed data, we use an exponential trend filter, and for motor current and torque command voltage data, we use a moving average filter. Both the filters can be found in Equations (19), and (20), respectively.

$$y(t) = a \times (e^{-(b \times t)}) + c \quad (19)$$

$$\text{Moving Average} = \frac{A_1 + A_2 + \dots + A_n}{n} \quad (20)$$

In Equation (18), unknown constants are a, b, c are required to be estimated to fit the exponential trend of the dataset. The values of unknown constants in the equation are found by using `curve_fit` function from Python library SciPy. Initially, all the constants' values are set to 1 and then using nonlinear least square optimization, the `curve_fit` function estimates the values of the unknown constants fitting an exponential trend to reaction wheel speed (ω_m) dataset. . In Equation (20), n is the window size for the calculation of moving average, and all the A terms are the values of data point.

3.4.1 Adjusting Hyperparameters

Adjusted hyperparameters for multivariate LSTM network during HI parameter prediction are listed in Table 6:

Table 6 – Tuned parameters for k_t prediction

Parameter	Value
Train to total data ratio	70%
Optimizer	ADAM
Initial learning (LR) rate	0.01
LR decrement per 10 epochs	85%
Validation split	25%
Batch size	24
Degree of differencing (L_B)	1
Number of epochs	300
Number of future data Prediction	100,000
Number of total data points in each feature	150,000
Data normalization	No
Data sampling rate	0.1 second

3.4.2 Monitoring Model's Learning Progression:

It is necessary to monitor the model's loss to understand if the employed network is learning the pattern for future prediction. We monitor both mean squared error loss that is calculated in the model training session and the validation loss using validation data. The model is learning if the loss and validation loss is converging to each other. The learning of LSTM network employed for state prediction in stage 1 is shown in the Figure 9, Figure 10, and Figure 11. The learning of multivariate LSTM network for forecasting HI parameter can be found in Figure 12.

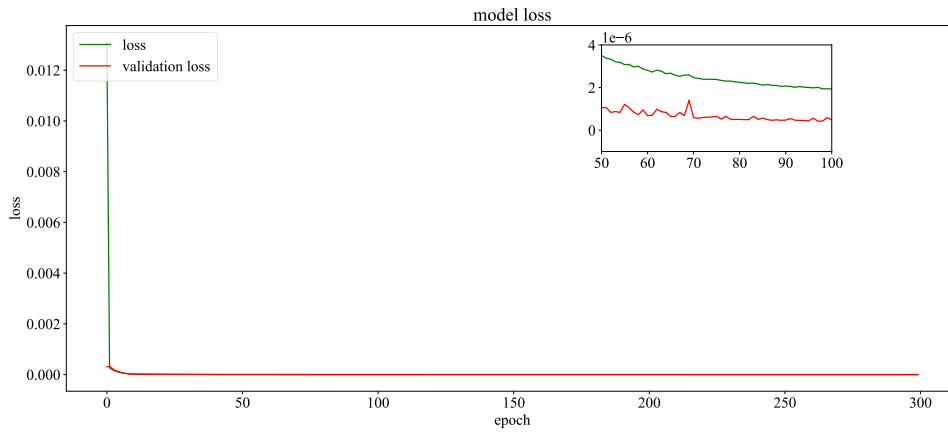


Figure 9. Graph of epoch vs loss for fitting the model to RW speed data

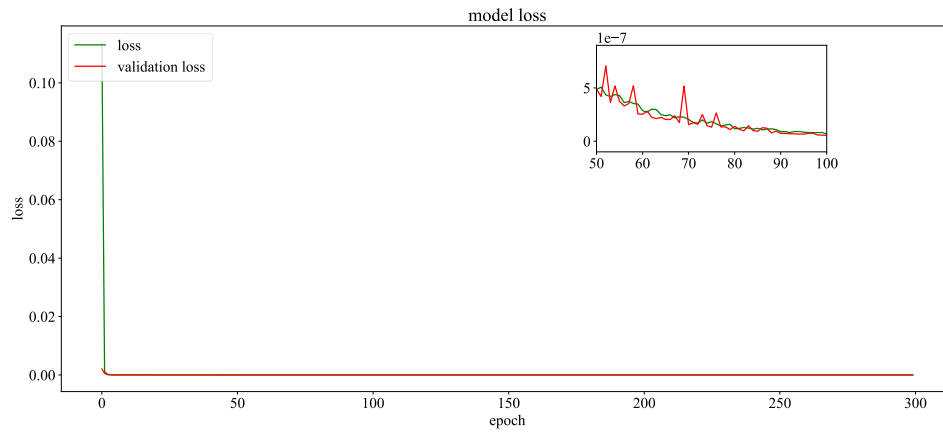


Figure 10. Graph of epoch vs loss for fitting the model to motor current data

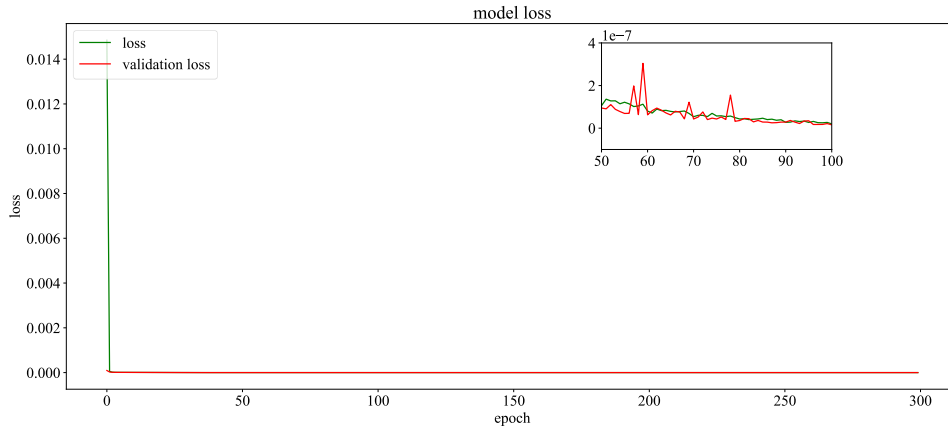


Figure 11. Graph of epoch vs loss for fitting the model to torque command voltage data

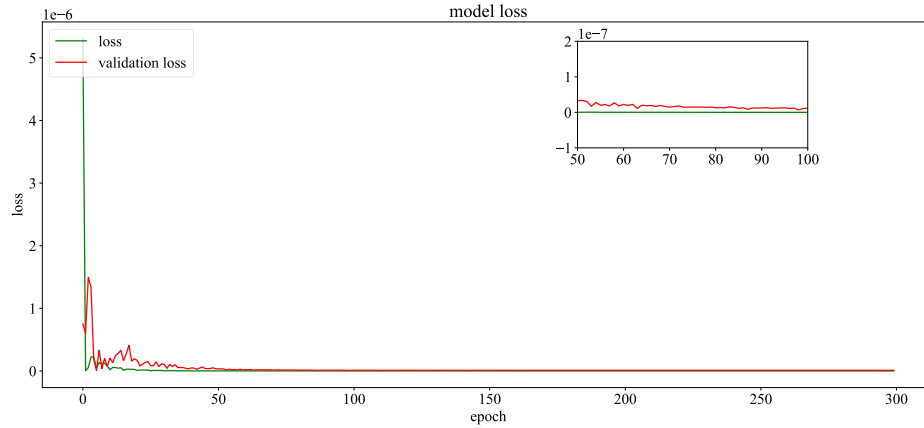


Figure 12. Graph of epoch vs loss for fitting the model to forecast HI parameter

3.5 Calculation of RUL (Stage 3)

The remaining useful life is calculated based on the predicted value of the HI parameter (k_t) and a threshold value for it. As stated in [2], [54], the threshold is based on the nominal value of motor torque (k_t). If the degraded value of k_t reaches 30 percent of its healthy state value, the system failure occurs. So, the intersection between the degradation data of the HI parameter and the threshold will show the point of predicted failure occurrence. The time window can be calculated from the present to the point of predicted failure to find out the RUL of the RW with incipient fault.

CHAPTER 4

CASE STUDY: REACTION WHEEL ONBOARD SATELLITE

4.1 Introduction

Prognosis is an unquestionable requirement for a large portion of advanced electromechanical machinery. Legitimate prognostics of a system can reduce the use of additional hardware for reliability purposes and, consequently, save production expenses and assembly intricacies. Forecasting is certainly not a simple task when working with a lot of variables and uncertainties. The issue can be addressed in mainly two ways, data-driven or model-based. A model-based technique is very accurate but only desirable if it is small and all the parameters are known. However, building a comprehensive model-based strategy is very arduous for a complex system. Henceforth, data-driven strategies are acquiring prevalence over the long haul. The focus of this study is to develop an optimized prognostic model for an RW in the attitude control system of a satellite to increase the reliability of the service.

4.2 ACS

The attitude control system (ACS) in an onboard satellite has two main types of components namely, actuators and sensors. The actuators are necessary to exert forces and torques while sensors collect all the measurements. There are two types of sensors in ACS: active and passive. The passive sensors do not have any internal processors, whereas active sensors contain internal processors. The common passive sensors are named in Figure 13 [55]:

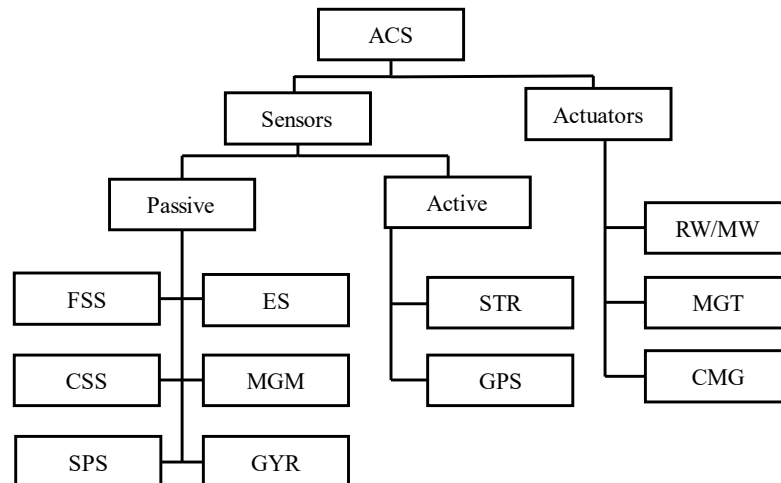


Figure 13. Satellite attitude control system units

where FSS stands for Fine Sun Sensor, CSS stands for Coarse Sun Sensor, SPS stands for Sun Present & Sun not Present, ES stands for Earth Sensor, MSM stands for Magnetometers, GYR stands for Gyroscope, STR stands for Star Sensor, GPS stands for Global Positioning System, RW stands for Reaction Wheel, MW stands for Momentum Wheel, MGT stands for Magnetorquers and CMG stands for Control Moment Gyros.

Here, in the attitude control system, FSS and CSS measure the direction of the sun line accuracy. SPS informs sun is present or not present. ES measures the earth's direction. MGM measures the direction of the earth's magnetic field. GYR measures the inertial angular rate of the satellite. The position of several stars is measured by STR. RW provides the torque necessary for three-axis orbit control. Constant torque is provided by MW using a constant speed rotary wheel. Control torque is generated by MGT. Finally, CMG is a gimbaled RW that serves a similar purpose as RW.

4.3 Reaction Wheel

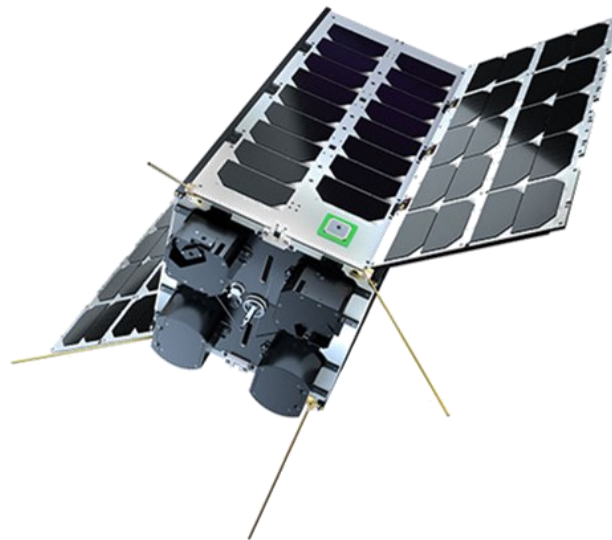


Figure 14. 16U nanosatellite bus M16P / M16P-R [1]

Figure 14 shows a nanosatellite with RW for three-axis attitude control. A reaction wheel is a flywheel generally used in machinery to preserve momentum. In the case of the satellite, the reaction wheel is used to rotate the satellite on its axis using Newton's third law of motion. The main components of a reaction wheel are an electronic motor, bearings, and a flywheel where most of its mass is located at its rim. Figure 15 shows an uncovered reaction

wheel and the disk at the top of the figure is the rotary wheel of the RW that contains most of its mass. The mathematical modelling of the reaction wheel that is used during this research is detailed in section 1.4. Reaction wheels are most commonly used in attitude control system of a small satellite. It helps the satellite to rotate around its axes without needing any propellant. Generally, solar power is used to drive the motor of an RW.



Figure 15. Reaction wheel unit from SSDC lab at Ryerson University. [2]

Studies [6], [56] show that for RWs, most faults happen in the bearing assembly (BA) with the briefest life span. Deficient or inadequate lubrication results in a faulty BA. As a result, the differential frictional torque will be affected. Subsequently, it should be monitored for changes in the system. However, it is not readily available for measurement and needs to be reproduced based on observable measurements in the system.

4.4 Reaction Wheel Assembly

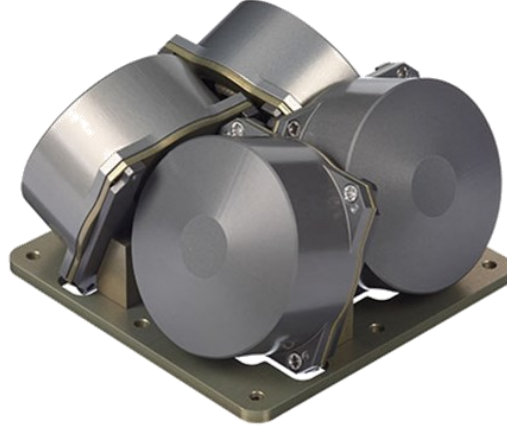


Figure 16. CubeSat Reaction Wheels Control System Sat Bus 4RW0 [57]

Reaction wheel assembly can be formed and configured in different ways depending on the requirements and preference. In Figure 16 a standard four-wheel configuration is presented. Each actuators torque contribution to each principal axis of the spacecraft body can be expressed by the following equations [2]:

$$\begin{bmatrix} \tau_x \\ \tau_y \\ \tau_z \end{bmatrix} = A_{RW} \begin{bmatrix} \tau_{w1} \\ \tau_{w2} \\ \tau_{w3} \\ \tau_{w4} \end{bmatrix} \quad (21)$$

where, τ_x, τ_y, τ_z are the torques applied to the x, y, z-direction of the satellite, respectively, and τ_{w_i} is the resultant torque generated by each RW on its axis. A mapping matrix (A) is used to map the two most popular configurations of setting up RW in the ACS: (1) Standard four-wheel configuration with three orthogonal RWs and one redundant oblique RW, and (2) four RWs in a pyramid configuration. The mapping matrix (A) can be expressed by Equation (22)

$$A_{RW_1} = \begin{bmatrix} 1 & 0 & 0 & -c\beta s\alpha \\ 0 & 1 & 0 & -c\beta s\alpha \\ 0 & 0 & 1 & s\beta \end{bmatrix} \quad (22)$$

$$A_{RW_2} = \begin{bmatrix} c\beta s\alpha & -c\beta s\alpha & -c\beta s\alpha & c\beta s\alpha \\ -c\beta c\alpha & -c\beta c\alpha & c\beta c\alpha & c\beta c\alpha \\ s\beta & s\beta & s\beta & s\beta \end{bmatrix}$$

where, A_{RW_1} , and A_{RW_2} are mapping matrix for configuration (1), and (2) respectively. Math function $\sin(\cdot)$ and $\cos(\cdot)$ are abbreviated as $c(\cdot)$ and $s(\cdot)$ respectively, α and β are in-plane angles and out-of-plane angles. A detailed explanation of these matrices can be found in [2]

4.5 Raw Data Collection and Preparation

As stated in section 3.2, synthetic data is generated using a mathematical model due to the unavailability of data real source. Later, to imitate the data from a real source missing data and noise are added before training the regression model. The different features of collected data are shown in Figure 17

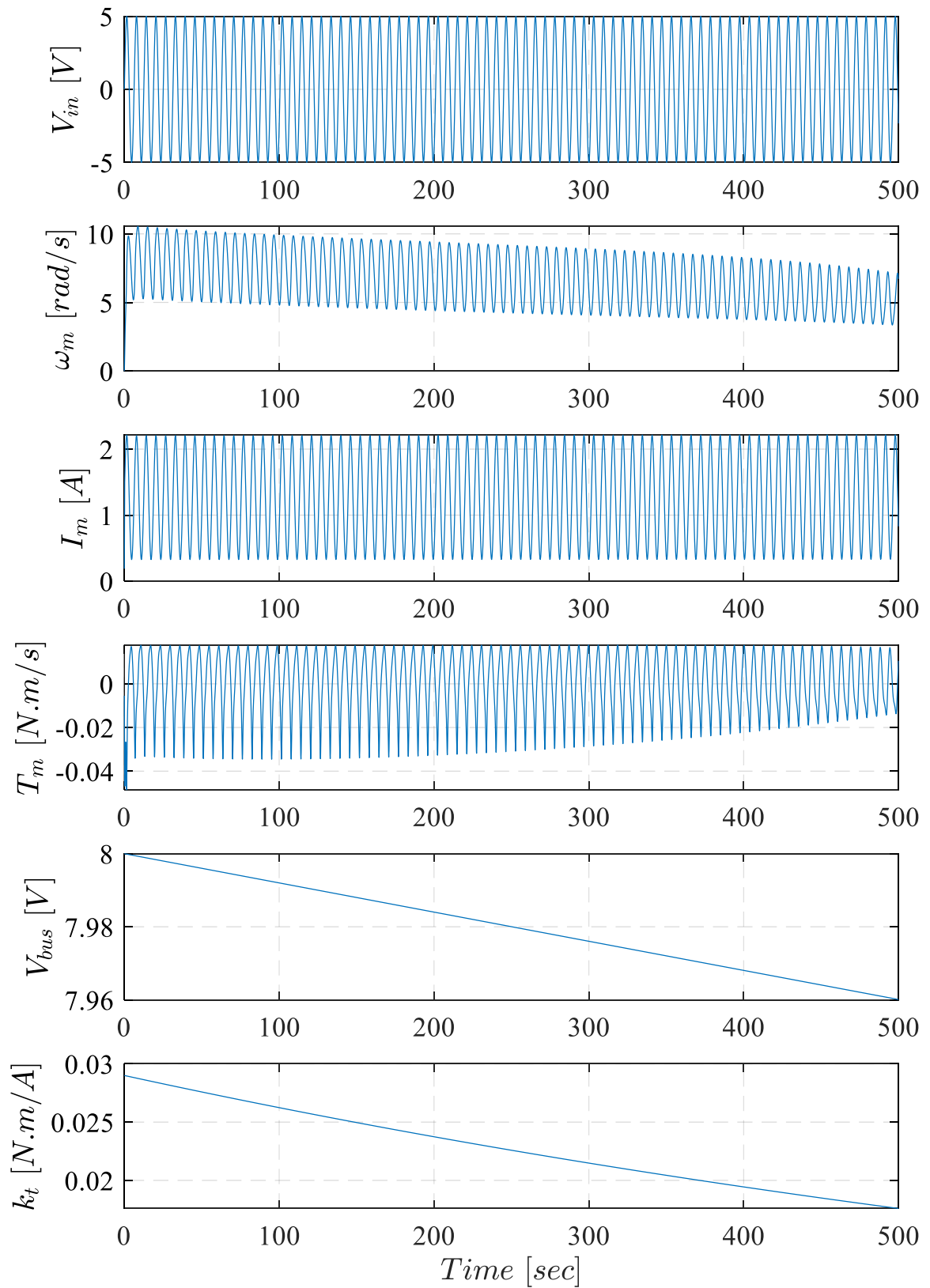


Figure 17. Raw dataset sample

4.6 Regression models for prognosis

The available state parameters from the sensor measurements are angular speed (ω_m), Motor current (I_m), and torque command voltage (V_{comm}). Then as stated in section 3.4 with the help of a regression model the future state of these parameters is predicted. Various regression methods (AR, ARMA, ARIMA, LSTM) have been used to determine the best fit model for the prediction of state parameters, and LSTM was found to be better suited [11]. Then, Motor torque (k_t) is defined as the HI parameter. Finally, with the help of second regression model (multi-variate LSTM) and the state parameters angular speed (ω_m), Motor current (I_m), and torque command voltage (V_{comm}) the future data of HI parameter is predicted as detailed in section 3.5.

CHAPTER 5

RESULTS AND DISCUSSION

The dataset is generated using a computer simulation in MATLAB, and the simulation is carried out on a dell computer with an Intel® Core™ i7-4790 CPU with a processing power of 8GHz, Intel® HD Graphics 4600, and 8 GB of RAM. For forecasting future system measurement data, an LSTM network from Python library Keras is used, and for state parameter prediction, a multi-variate LSTM network is employed. The LSTM network employed for forecasting system measurement is known as vanilla LSTM. This network has an input layer, a visible layer, a hidden layer with four LSTM blocks, and an output layer. The input layer of this network takes three-dimensional array as input, where the first dimension is the batch size, second dimension is the time step, and the third dimension is number of units in one input sequence. The employed multivariate LSTM network HI parameter prediction takes multiple features as input and returns a single output. In this case, the network takes ω_m, I_m, V_{comm} as input and returns HI parameter k_t as output. The tuned hyperparameters for the LSTM network used in stage 1 can be found in Table 5 and in the Table 6 the tuned hyperparameters for multivariate LSTM network are listed.

5.1 State Prediction (Stage 1)

In this stage, with the use of a suitable regression model, we predict the future state of the available measurements, angular speed (ω_m), Motor current (I_m), and torque command voltage (V_{comm}). Multiple methods are employed for state prediction to find out the best fit method to predict the future state available measurements. Among the method, the results from an ARIMA model and an LSTM network are discussed in this section as they provide very promising regression accuracy for the time series dataset.

5.1.1 State Prediction with ARIMA model

Figure 18 true reaction wheel data is plotted against time. From the diagram, it is visible that the time series is nonstationary. So, a differencing order of 1 is selected to make the dataset stationary for the ARIMA model to learn the pattern. Understanding true data patterns is important as it helps to make an initial guess for the ARIMA model hyperparameters, lag order (p), degree of differencing (d), and order of moving average (q). A detailed explanation of this parameter can be found in section 2.1. Figure 18 also shows that for this

particular dataset there is a significant change in magnitude of the y-axis value till 40 seconds then the RW speed seems to be stabilizing. So, it makes the job of splitting the dataset into train and test segments very tricky.

In order to find a suitable lag order p , an autocorrelation graph is plotted in Figure 19. Where in the graph we can see a positive correlation for the first 430 (approximately) lags. The plot also shows that the decrement is very significant for the first 250 lags. However, selecting a higher lag order increases computational complexity, and it also does not always provide a better result. In practice, for this dataset, taking a lag order value greater than 5 does not yield any result as the model fails to converge in the available computational resources. Hence a lag order of 2 is selected. The model accuracy results in Table 8 also justify the fact of choosing smaller lag order.

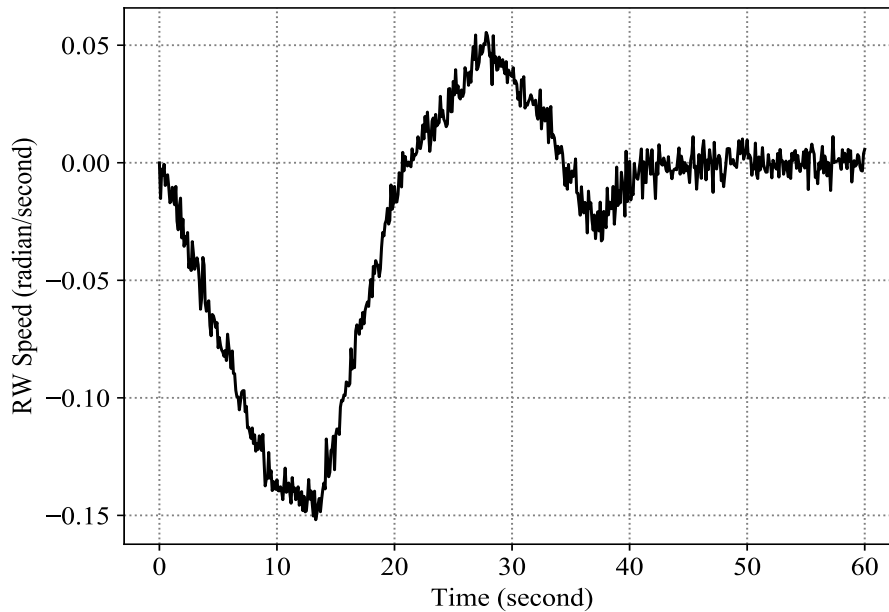


Figure 18. True RW speed data plotted against time

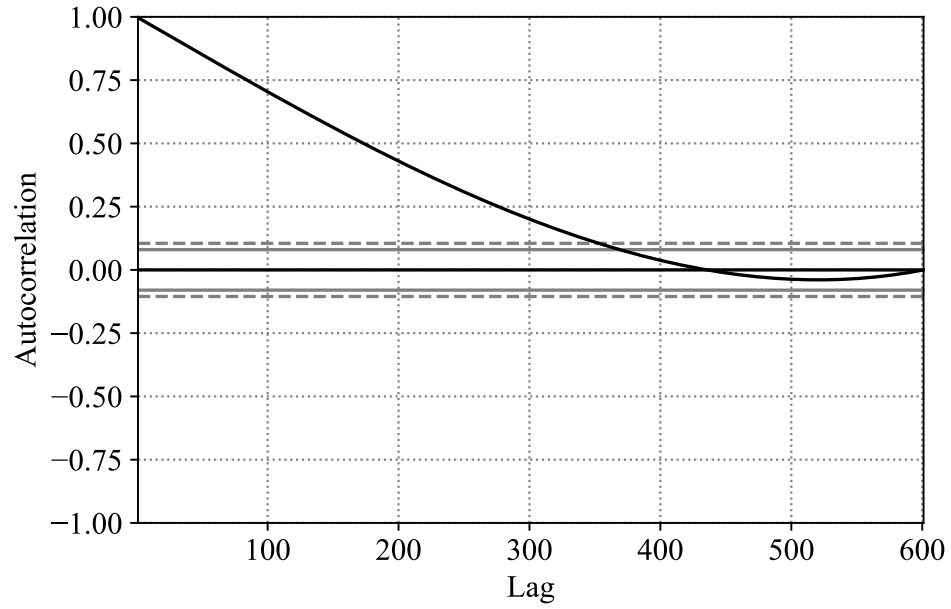


Figure 19. Autocorrelation vs lag order of the dataset

To resemble the data from real sources, white Gaussian noise is added to the dataset as shown in Figure 20. In the figure red, blue, and black line represents the noisy dataset after addition of white Gaussian noise, the true data, and added noise respectively. Here, the added noise has a signal-to-noise ratio of 51.84 dB and the signal-to-noise ratio is calculated as detailed in section 3.2.

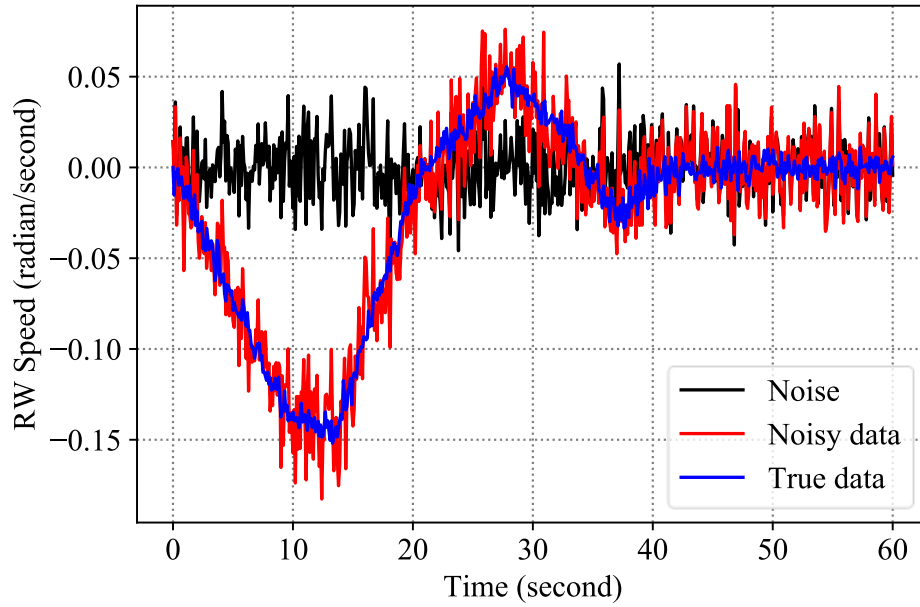


Figure 20. Adding white gaussian noise to the RW speed dataset

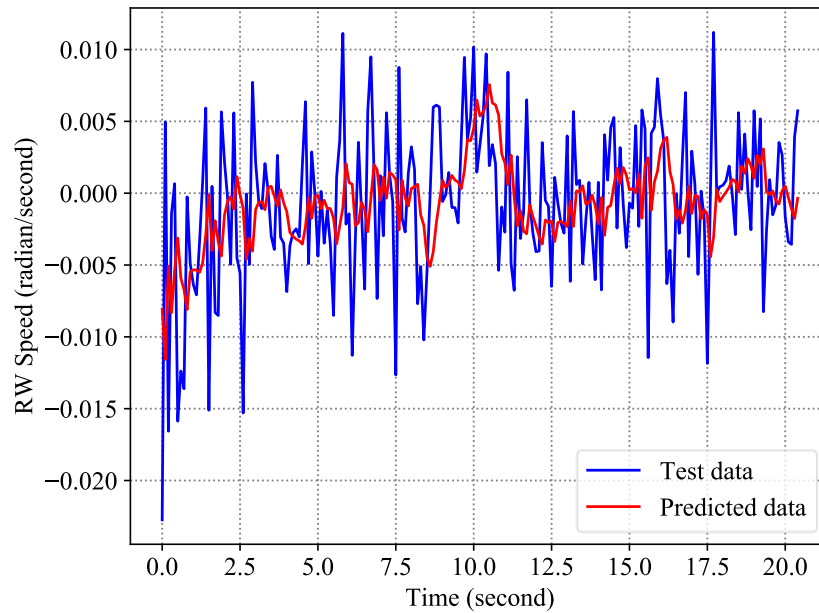


Figure 21. RW speed data (test segment) prediction with ARIMA model

In Figure 21, the predicted test data and true test data of the RW speed dataset are plotted against time. The blue and red line represents true test data and predicted data respectively. Here test dataset length is 34% of the total data. The predicted data clearly follows the pattern of the true dataset and the obtained error for this setup is NRMS 0.167

In Table 7 the error of test data prediction with ARIMA model and relative train set ratio of test dataset (TSROTD) is listed. The accuracy of the model is listed as the normalized root mean squared error of the model prediction in the test dataset of RW speed data. Even though the accuracy is promising, but it is not enough for a regression model where higher precision is required.

Table 7 – Impact of training set size on the accuracy of the model

TSROTD	NRMS of Test Prediction
66%	0.167
75%	0.188
85%	0.138

To get the best prediction result, the ARIMA model parameters p , d , q values need to be adjusted properly. A detailed explanation of these ARIMA model parameters can be found in section 2.1. In Table 8 the ARIMA model accuracy concerning the respective p , d , q values is listed. The accuracy is calculated as a mean squared error (MSE) and normalized root mean squared error (NRMS) of the prediction in the test dataset of RW speed data.

Table 8 – MSE and NRMS respective to p , d , q values in ARIMA

p, d, q	MSE	NRMS
5,1,0	0.006	0.176
2,1,0	0.006	0.178
2,1,2	0.006	0.167
2,1,1	0.006	0.175
1,0,1	0.006	0.175
5,1,1	0.006	0.174
5,1,0	0.006	0.175
2,0,2	0.006	0.171
1,1,1	0.006	0.174
2,0,0	0.006	0.184

5.1.2 State Prediction with LSTM Network

Figure 23 shows predicted reaction wheel speed (ω) states. The magnified axis in Figure 234 shows a staircase effect in train and test predictions. However, the prediction successfully follows the sinusoidal and exponential declination of the true dataset. The model is tested with different sampling rates, and the model performance is robust when the model hyperparameters (learning rate, batch size, number of epochs, and the size of train, test, and validation dataset) are adjusted properly. Table shows, for the RW speed predictions, the model accuracy is better for higher frequencies, and it tends to be degrading for lower frequencies. However, for real-life applications, the use of higher frequency has some drawbacks, and lower frequency is preferred due to higher penetration capability [58]. During other sensitivity analyses and RUL calculations in, we have used input frequency 0.1 Hz for sensor data collection.

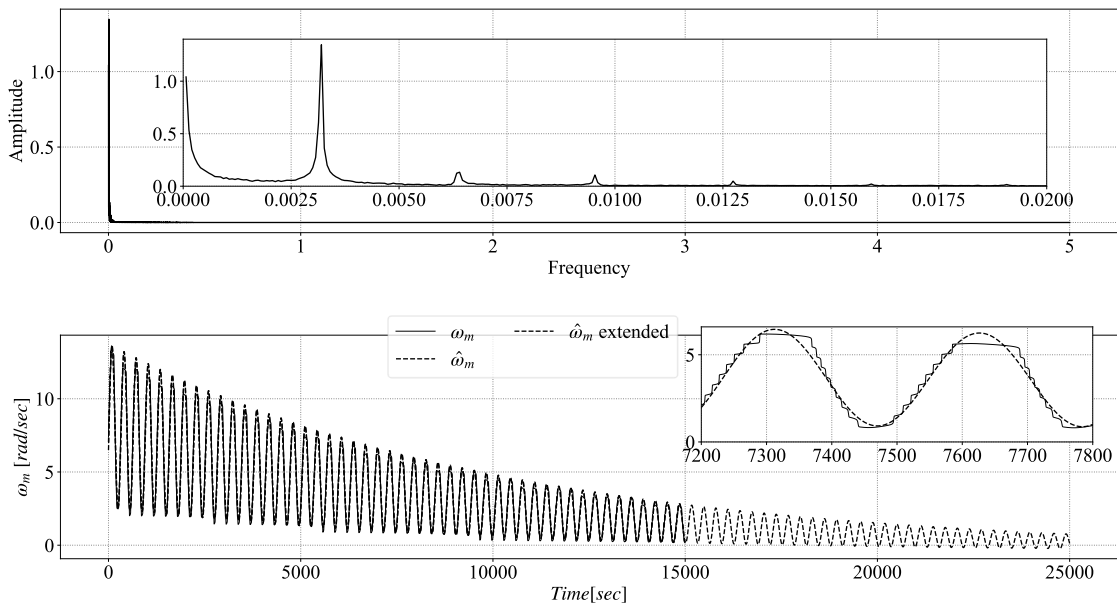


Figure 22. Fitting reference line for RW speed (ω) prediction

Figure 22 shows the fitted reference line that is used as a base when predicting data in future time step. This allows the model to deal with the conventional problem of prediction model divergence with time when working with a nonstationary time series.

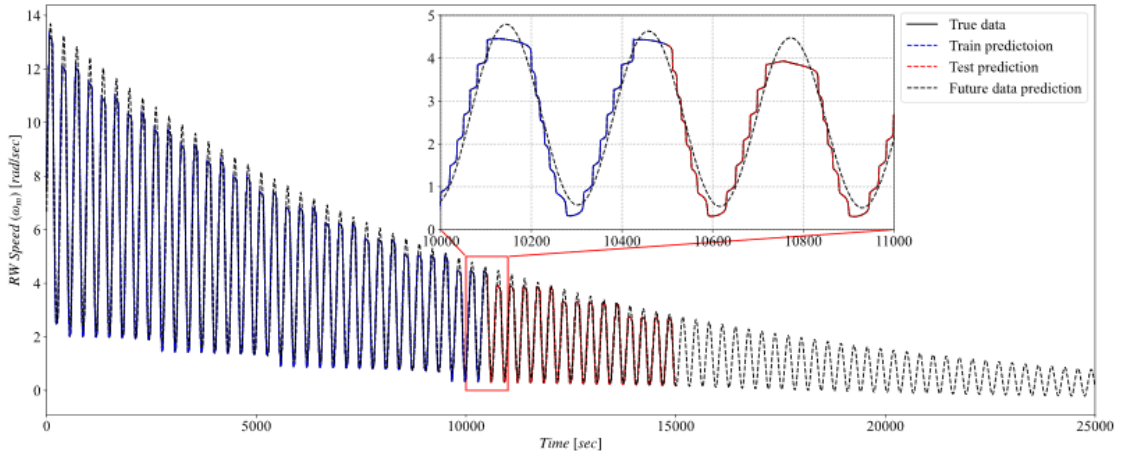


Figure 23. Prediction of RW speed data

Figure 24 shows the prediction of motor current (I_m) data. As Figure 5 shows, the model almost accurately predicts the motor current. We obtain prediction NRMS error 0.01 for motor current data.

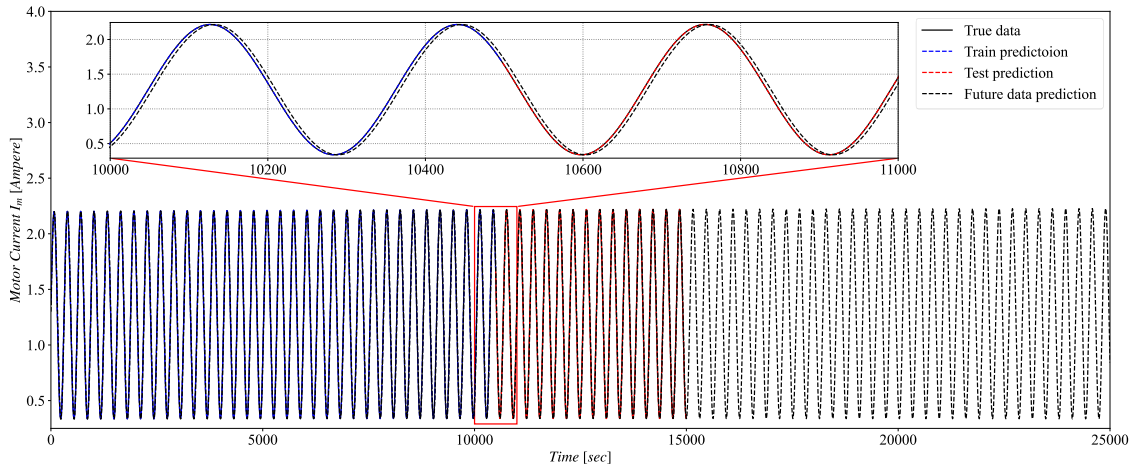


Figure 24. Prediction of motor current data

Figure 25 shows the prediction of torque command voltage (V_{comm}). The prediction in the figure shows that it follows the true data in the test segment perfectly and can predict future data with considerable good accuracy. We obtain forecasting NRMS error 0.01 for torque command voltage data.

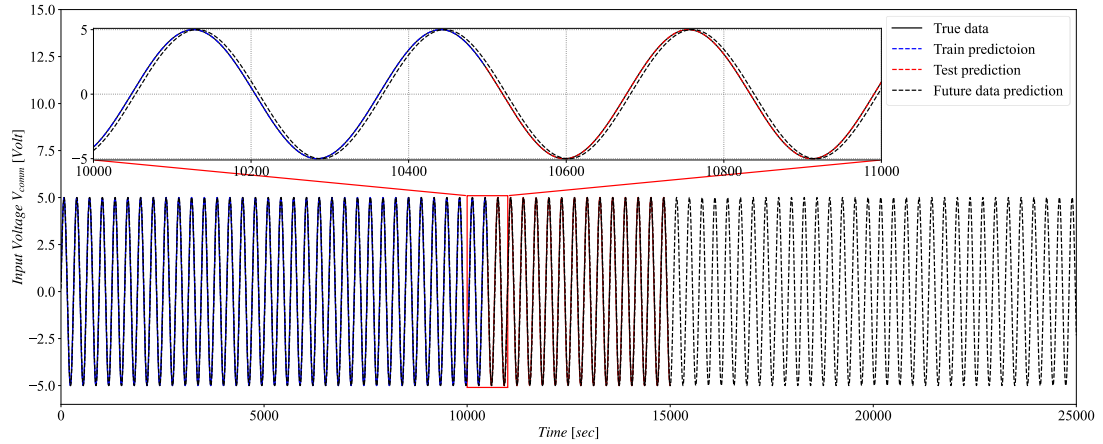


Figure 25. Prediction of torque command voltage data

5.2 HI Parameter Prediction (Stage 2)

Figure 26 shows the motor torque coefficient (k_t) predictions. As Figure 26 shows, the prediction very closely follows the model-generated motor torque data. We obtain NRMS 0.02 for forecasting motor torque data. However, with the increase in time, there is a slight divergence from the true data. This happens because the uncertainty of the prediction increases with time. When predicting much further in the future even a minor error in prediction of the first time step will propagate through a time when making predictions over predicted data.

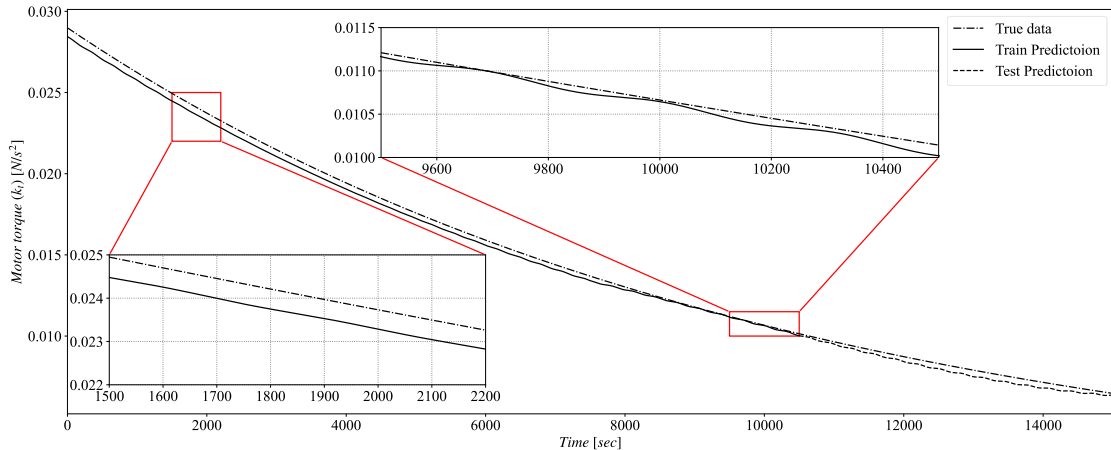


Figure 26. Prediction of HI parameter (k_t)

5.3 Calculation of RUL (Stage 3)

Figure 27 shows the confidence interval and a threshold line for the HI parameter to determine the RUL of the RW. The confidence is very narrow, and the model has a good prediction accuracy with normalized root mean squared error (NRMS) 0.02. However, note that when predicting the future data, the prediction is based on the prediction of the previous time step. Therefore, the error gets propagated even if there is a minor error in prediction. The prediction points out the system failure at 11,800 seconds from the beginning of the simulation, and the true data almost shows the same failure time in the diagram. The threshold is drawn from historical data. Nearly at 30 percent of the initial value of k_t , the system fails to perform properly [45]

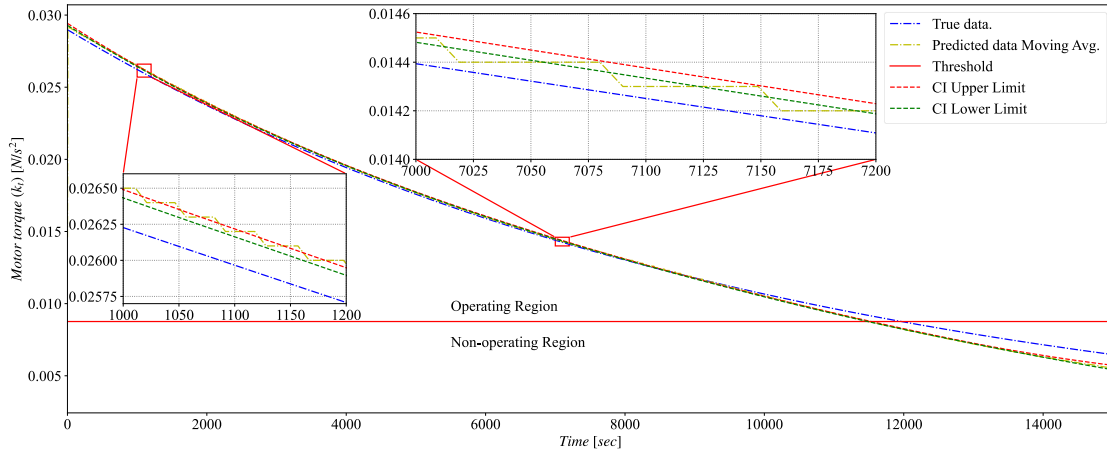


Figure 27. Confidence boundary of predicted HI parameter and RUL

5.4 Sensitivity Analysis

To perform robustly in real-life applications, the model needs to perform under different conditions, including variations in missing data, noise, different input frequencies in the data, and data sampling rate. For the proposed model, an interpolation technique is efficient enough for addressing the missing data issue, as shown in Table 9 and Figure 28.

Table 9 – Missing data imputation accuracy for RW speed data

Each cell probability of missing value (%)	Accuracy of prediction (NRMS)
5	0.01
10	0.02
15	0.02
20	0.02
25	0.04
30	0.05

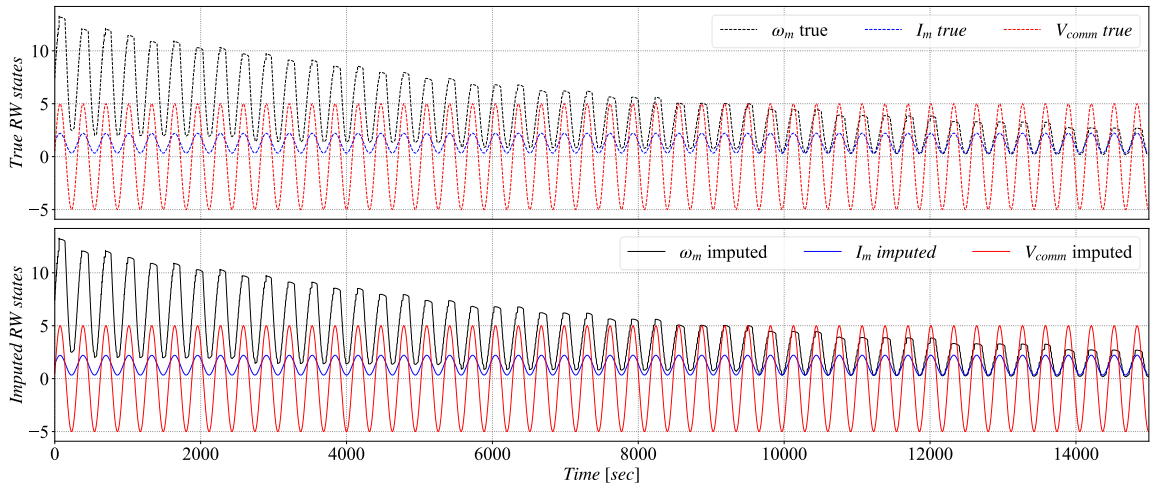


Figure 28. missing data imputation for 35% ratio of missing.

The accuracy of the model is measured in a normalized root mean squared (NRMS) error for the test dataset. Table 10 shows that for RW speed prediction, the model accuracy is better for higher frequencies and tends to be degrading for lower frequencies. However, for real-life applications, the use of much higher frequency has some complications. We have used input frequency for sensor data collection during other sensitivity analyses and RUL calculations we have used input frequency 0.1 Hz for sensor data collection.

Table 10 – Model accuracy for different frequencies in the input dataset

Frequency in the input dataset (rad/sec)	Test NRMS (RW speed)	Test NRMS (Motor Current)	Test NRMS (Torque Command Voltage)
1.0	0.01	0.01	0.01
0.5	0.02	0.01	0.01
0.1	0.01	0.01	0.01
0.07	0.02	0.01	0.01
0.05	0.01	0.01	0.01
0.03	0.02	0.01	0.01
0.02	0.02	0.01	0.01
0.01	0.01	0.02	0.01

Figure 29 shows a noisy dataset pattern of RW speed data. White Gaussian noise is added to the RW speed data. The added noise amount, in this case, is 25.20 dB and it is expressed as a signal-to-noise ratio (SNR). The calculation process of SNR is detailed in section 3.2. The prediction of future RW motor speed data using noisy dataset of is plotted against time in Figure 30.

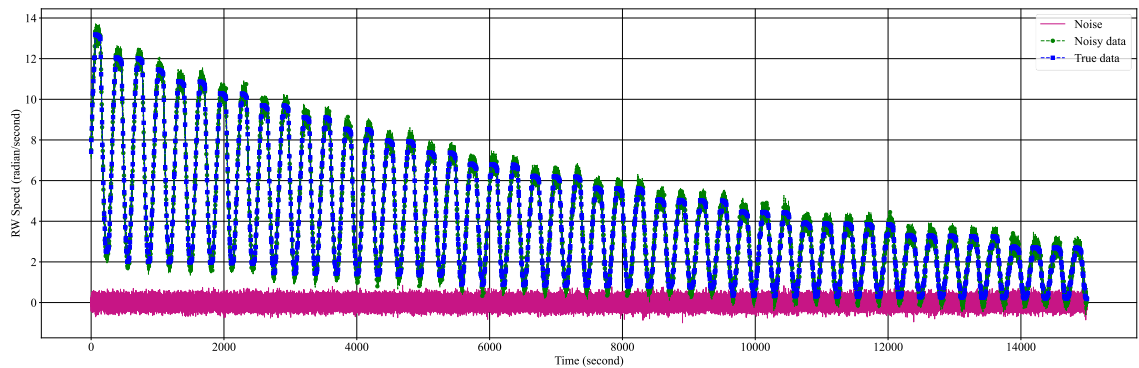


Figure 29. Adding noise to RW speed data

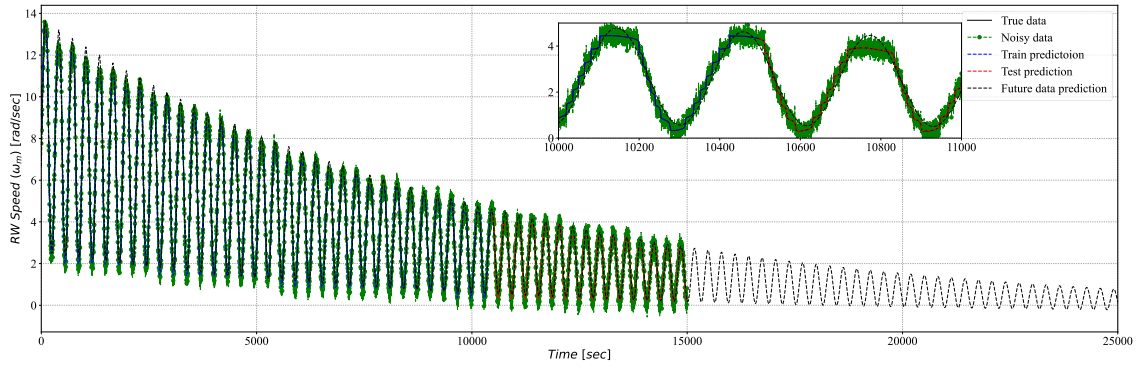


Figure 30. Prediction of RW speed data based on noisy dataset

In Figure 31 noisy dataset of motor, current is available. Here 68.34 dB noise is added with the true data of motor current. The prediction on noisy motor current data is shown in Figure 32.

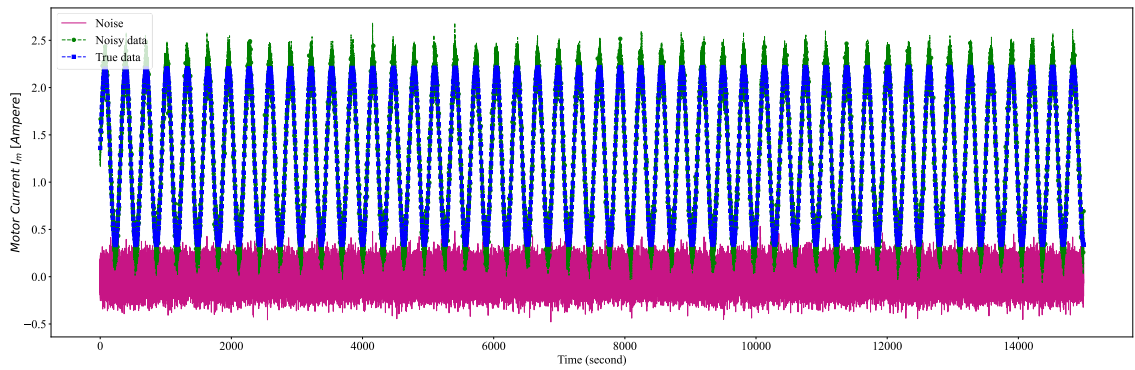


Figure 31. Adding noise to motor current

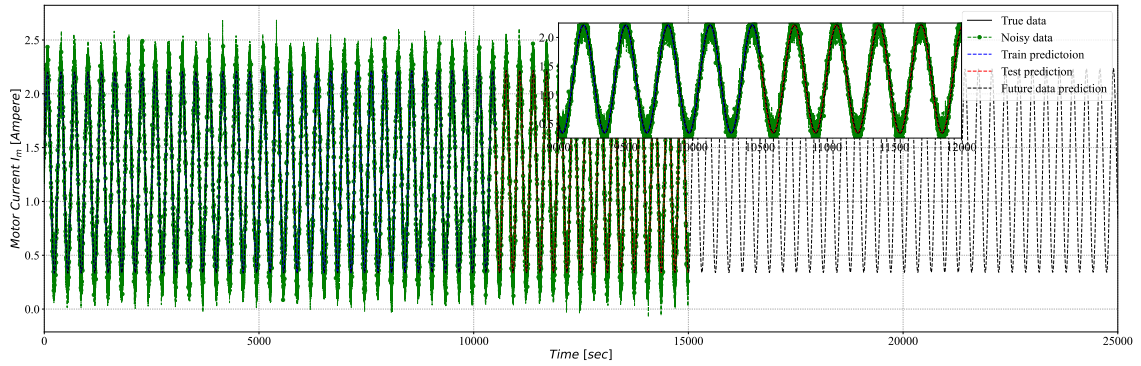


Figure 32. Prediction on noisy motor current data

56.44 dB noise is added with the true data of torque command voltage and the outcome of noisy torque command voltage data is plotted against time in Figure 33. As it is shown in the figure blue line is the noisy torque command voltage data. . The prediction on noisy torque command voltage data is shown in Figure 34.

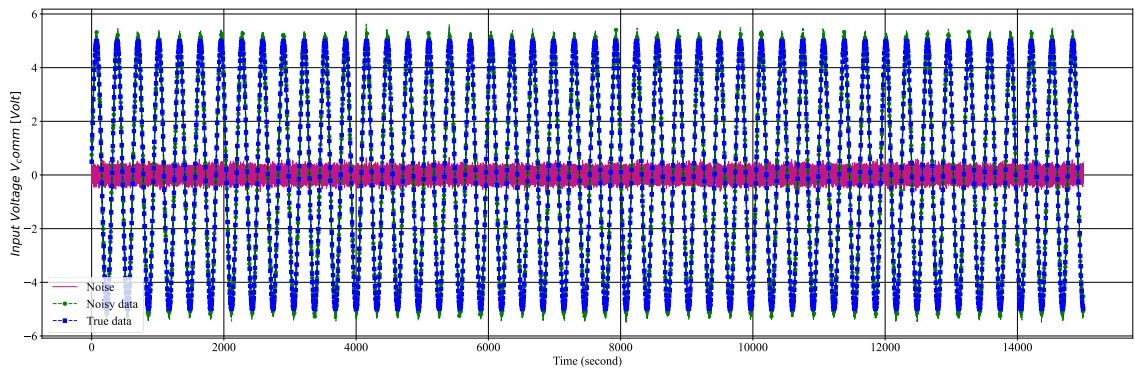


Figure 33. Adding noise to the torque command voltage

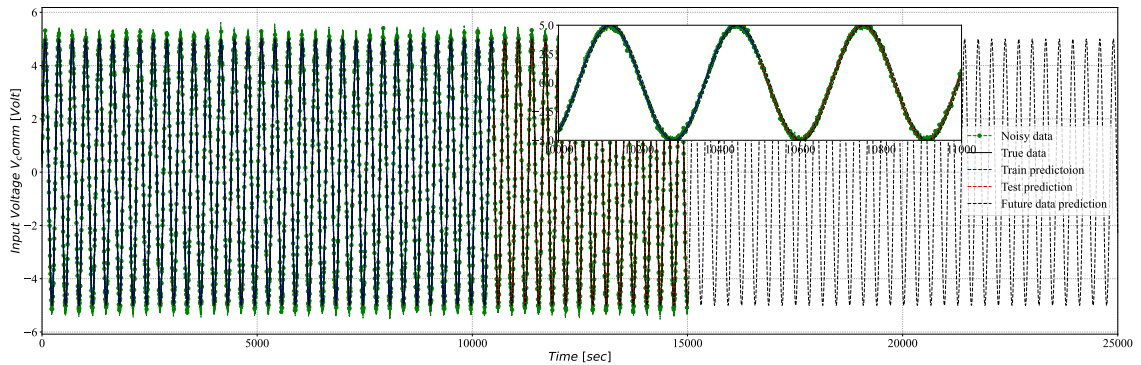


Figure 34. Prediction of torque command voltage based on noisy data

279.69 dB noise is added with the motor torque data to form noisy motor torque data and the noisy data, the added noise, and the true data is plotted against time in Figure 35. As shown in the figure green line represents noisy motor torque data.

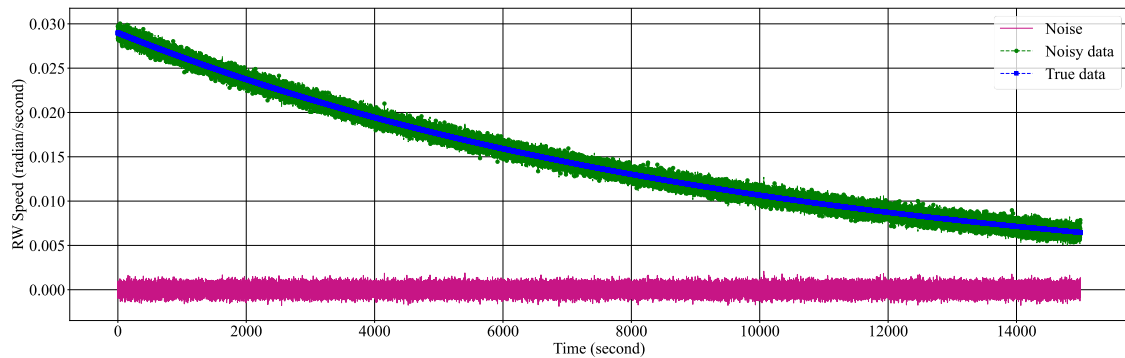


Figure 35. Adding noise to the motor torque coefficient data

Table 11 shows the model performance under the influence of added Gaussian white noise in the input data. As Table 11 shows, the model performance is very robust, and it can handle minor to medium noise in the input data without compromising the model accuracy. However, the model performance degrades with the introduction of higher noise levels in the input dataset.

Table 11 – Model performance degradation for different noise level

Serial No.	Noise in ω (dB)	Noise in I_m (dB)	Noise in V_{comm} (dB)	Noise in k_t (dB)	Prediction NRMS (Test Data)
01	0	0	0	0	0.02
02	147.58	166.9	170.23	161.11	0.02
03	131.36	150.68	154.01	144.09	0.02
04	130.65	145.82	133.36	130.68	0.02
05	92.13	111.45	114.78	105.65	0.04
06	55.47	74.8	78.12	69.00	0.04
07	27.75	47.7	50.40	41.28	0.07
08	11.53	30.85	34.18	25.06	0.34

Further sensitivity analysis is carried out for larger dataset with less severe incipient fault. The methodology for this is same as the one described in the methodology section of this document, and the only difference is it requires higher computational support. The tuned hyperparameters for HI parameter prediction and RUL estimation using day scale dataset is listed on Table 12 ,and for the month scale dataset listed on Table 13

Table 12 – Tuned parameters and model inputs for k_t prediction using day scale dataset

Parameter	Value
Train to total data ratio	70%
Optimizer	ADAM
Initial learning (LR) rate	0.01
LR decrement per 10 epochs	65%
Validation split	25%
Batch size	128
Degree of differencing (L_B)	1
Number of epochs	250
Number of total data points in each feature	1,400,000
Data normalization	No
Data sampling rate	1 second

Predicted HI parameters for for day scale datasets is plotted in Figure 36. The NRMS error in the prediction is 0.01.

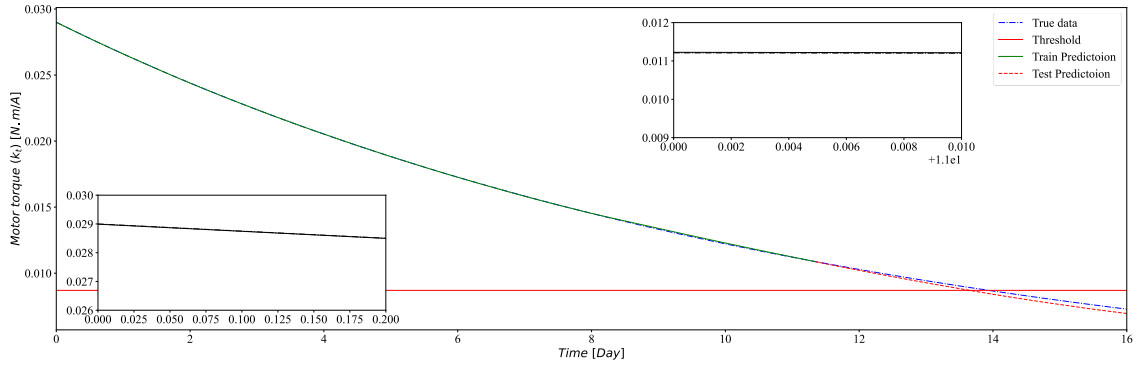


Figure 36. Prediction of Hi parameter using day scale dataset

Table 13 – Tuned parameters and model inputs for k_t prediction using month scale dataset

Parameter	Value
Train to total data ratio	75%
Optimizer	ADAM
Initial learning (LR) rate	0.01
LR decrement per 10 epochs	65%
Validation split	25%
Batch size	256
Degree of differencing (L_B)	1
Number of epochs	300
Number of total data points in each feature	6,600,000
Data normalization	No
Data sampling rate	2 second

The NRMS error for prediction of HI parameter for this set up using month scale data is 0.02. The predicted HI parameter, and the threshold is plotted in Figure 37 for calculation of RUL.

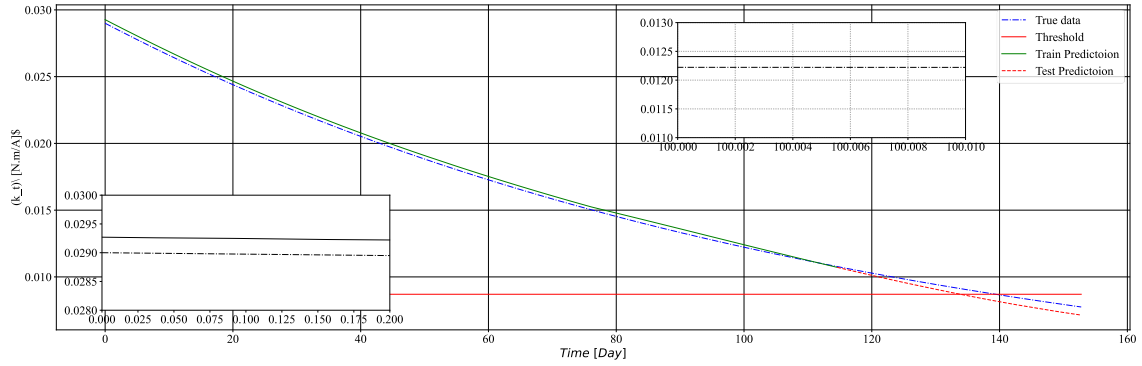


Figure 37. Prediction of HI parameter using month scale dataset

CHAPTER 6

CONCLUSIONS AND FUTURE WORKS

6.1 Conclusions

This study proposes a three-step prognosis technique for calculating RUL of the RW under incipient fault. A version of the recurrent neural network, LSTM, is used for predicting the future of the system measurements. Using a multi-variate LSTM network, we predict the RW health index parameter (k_t). From the threshold of the HI, we calculate the RUL of the RW. The state prediction data shows, the LSTM model lands superior accuracy to ARIMA model. The goal of this research is to propose a complete prognostic model for satellite reaction wheel. So, in this research more optimization to the LSTM network is done to reduce the computational time and enhance the accuracy. Some sensitivity analysis result also show the the robustness of the model against missing data or noise challenge in real-life application. Other neural networks and models can be tried to solve following the same procedure addressed here in further extension of this study. The proposed model uses simulation data because of difficulty to access data from a reaction wheel in service.

The procedure is straightforward and robust under noise, missing data, and different input frequencies. However, when predicting the future data, The predictions are carried out based on the prediction in the previous time step. Therefore, even a minimal error in prediction in the first step propagates to the next one making prediction for a larger time window unsuitable. The use of the proposed model can increase the reliability of the service by managing the scheduled maintenance time and reduce the possible downtime of the system. The proposed model has potential as it provides very high accuracy in prediction, and it also provides a comprehensive data-driven fault prognosis technique for reaction wheels, among other systems.

6.2 Future Works

Future works in this field can include training the model with the data from a real-life satellite in operation. In this study above a single fault, severity is, so there is provision for continuing the study to build a model that can address multiple fault scenarios with different fault severity at a time. Improved machine learning can be employed to enhance the accuracy of the regression analysis for state parameters and health index parameters of the

reaction wheel. The proposed model can be also used as a base model to follow and develop fault prognosis method for control moment gyros and other similar electro mechanical systems. However, the application of proposed model directly to another system may not yield a good result.

REFERENCES

- [1] B. Doncaster, C. Williams, and J. Shulman, “2018 Nano/Microsatellite Market Forecast, 8th Edition,” pp. 1–28, 2018, [Online]. Available: <http://www.spaceworkscommercial.com/wp-content/uploads/2018/04/Nano-Microsatellite-Market-Forecast-8th-Edition-2018.pdf>.
- [2] A. Rahimi, “Author’s Declaration,” Ryerson University, 2017.
- [3] A. Rahimi, K. D. Kumar, and H. Alighanbari, “Failure Prognosis for Satellite Reaction Wheels Using Kalman Filter and Particle Filter,” *J. Guid. Control. Dyn.*, no. 1, pp. 1–4, 2019, doi: 10.2514/1.G004616.
- [4] A. Rahimi, K. D. Kumar, and H. Alighanbari, “Fault estimation of satellite reaction wheels using covariance based adaptive unscented Kalman filter,” *Acta Astronaut.*, vol. 134, no. February, pp. 159–169, 2017, doi: 10.1016/j.actaastro.2017.02.003.
- [5] A. Barua and K. Khorasani, “Hierarchical fault diagnosis in satellites formation flight,” *Annu. Conf. Progn. Heal. Manag. Soc. PHM 2009*, pp. 1–16, 2009.
- [6] Jingfu Wang, Heng Zheng, Qin Li, Hang Wu, and Bo Zhou, “Prognostic for on-orbit satellite momentum wheel based on the similitude method,” in *2015 Prognostics and System Health Management Conference (PHM)*, Oct. 2015, pp. 1–5, doi: 10.1109/PHM.2015.7380085.
- [7] M. Rocchi *et al.*, “Fault prognosis for rotating electrical machines monitoring using recursive least square,” *EDERC 2014 - Proc. 6th Eur. Embed. Des. Educ. Res. Conf.*, pp. 269–273, 2014, doi: 10.1109/EDERC.2014.6924402.
- [8] G. Liu, D. Li, R. Zhang, J. Zhang, and Z. Z. Li, “Failure detection using matrix pencil algorithm to reaction wheel,” *Appl. Mech. Mater.*, vol. 29–32, pp. 1594–1601, 2010, doi: 10.4028/www.scientific.net/AMM.29-32.1594.
- [9] I. F. Diagnosis, *kitab in hepsini indir and Prognosis for Intelligent Fault Diagnosis and Prognosis for*. 2006.
- [10] A. Rahimi and A. Saadat, “Fault isolation of reaction wheels onboard three-axis controlled in-orbit satellite using ensemble machine learning,” *Aerosp. Syst.*, vol. 3, no. 2, pp. 119–126, 2020, doi: 10.1007/s42401-020-00046-x.
- [11] M. Sirajul Islam and A. Rahimi, “Use of A Data-Driven Approach for Time Series Prediction in Fault Prognosis of Satellite Reaction Wheel,” *IEEE Trans. Syst. Man,*

- Cybern. Syst.*, vol. 2020-Octob, pp. 3624–3628, 2020, doi: 10.1109/SMC42975.2020.9283435.
- [12] M. Sirajul Islam and A. Rahimi, “Fault Prognosis of Satellite Reaction Wheels Using A Two-Step LSTM Network,” *2021 IEEE Int. Conf. Progn. Heal. Manag.*, pp. 1–7, Jun. 2021, doi: 10.1109/ICPHM51084.2021.9486655.
- [13] X. Jin, Z. Que, Y. Sun, Y. Guo, and W. Qiao, “A Data-Driven Approach for Bearing Fault Prognostics,” *IEEE Trans. Ind. Appl.*, vol. 55, no. 4, pp. 3394–3401, 2019, doi: 10.1109/TIA.2019.2907666.
- [14] Y. Yun, J. Lee, H. Oh, and J.-H. Choi, “Remaining useful life prediction of reaction wheel motor in satellites,” *JMST Adv.*, vol. 1, no. 3, pp. 219–226, 2019, doi: 10.1007/s42791-019-00020-5.
- [15] T. Van Tung, B.-S. Yang, V. T. Tran, and B.-S. Yang, “Machine Fault Diagnosis and Prognosis : The State of The Art,” *Int. J. Fluid Mach. Syst.*, vol. 2, no. 1, pp. 61–71, Mar. 2009, doi: 10.5293/IJFMS.2009.2.1.061.
- [16] B. Zhang, L. Zhang, and J. Xu, “Degradation Feature Selection for Remaining Useful Life Prediction of Rolling Element Bearings,” *Qual. Reliab. Eng. Int.*, vol. 32, no. 2, pp. 547–554, 2016, doi: 10.1002/qre.1771.
- [17] A. Rohani Bastami, A. Aasi, and H. A. Arghand, “Estimation of Remaining Useful Life of Rolling Element Bearings Using Wavelet Packet Decomposition and Artificial Neural Network,” *Iran. J. Sci. Technol. - Trans. Electr. Eng.*, vol. 43, pp. 233–245, 2019, doi: 10.1007/s40998-018-0108-y.
- [18] S. Marble and D. Tow, “Bearing health monitoring and life extension in satellite momentum/reaction wheels,” *IEEE Aerosp. Conf. Proc.*, vol. 2006, pp. 1–7, 2006, doi: 10.1109/aero.2006.1656138.
- [19] T. Benkedjouh, K. Medjaher, N. Zerhouni, and S. Rechak, “Health assessment and life prediction of cutting tools based on support vector regression,” *J. Intell. Manuf.*, vol. 26, no. 2, pp. 213–223, 2015, doi: 10.1007/s10845-013-0774-6.
- [20] C. Liu, L. Zhang, J. Niu, R. Yao, and C. Wu, “Prognostics for rotating machinery using variational mode decomposition and long short-term memory network,” *Conf. Proc. - IEEE Int. Conf. Syst. Man Cybern.*, vol. 2019-Octob, no. 2018, pp. 7–12, 2019, doi: 10.1109/SMC.2019.8913840.

- [21] A. K. Mahamad, S. Saon, and T. Hiyama, “Predicting remaining useful life of rotating machinery based artificial neural network,” *Comput. Math. with Appl.*, vol. 60, no. 4, pp. 1078–1087, 2010, doi: 10.1016/j.camwa.2010.03.065.
- [22] M. Hamadache, J. H. Jung, J. Park, and B. D. Youn, “A comprehensive review of artificial intelligence-based approaches for rolling element bearing PHM: shallow and deep learning,” *JMST Advances*, vol. 1, no. 1–2, pp. 125–151, 2019, doi: 10.1007/s42791-019-0016-y.
- [23] A. Heng, S. Zhang, A. C. C. Tan, and J. Mathew, “Rotating machinery prognostics: State of the art, challenges and opportunities,” *Mech. Syst. Signal Process.*, vol. 23, no. 3, pp. 724–739, 2009, doi: 10.1016/j.ymsp.2008.06.009.
- [24] S. U. Kurse and S. Pradeep, “Prognosis of Rotating Machinery Using Artificial Neural Network [A Review],” *Ijert*, vol. 2, no. 8, pp. 1433–1439, 2013.
- [25] J. Lee, F. Wu, W. Zhao, M. Ghaffari, L. Liao, and D. Siegel, “Prognostics and health management design for rotary machinery systems - Reviews, methodology and applications,” *Mech. Syst. Signal Process.*, vol. 42, no. 1–2, pp. 314–334, 2014, doi: 10.1016/j.ymsp.2013.06.004.
- [26] G. W. Vogl, B. A. Weiss, and M. Helu, “A review of diagnostic and prognostic capabilities and best practices for manufacturing,” *J. Intell. Manuf.*, vol. 30, no. 1, pp. 79–95, 2019, doi: 10.1007/s10845-016-1228-8.
- [27] R. Hasani, G. Wang, and R. Grosu, “A machine learning suite for machine components’ health-monitoring,” *33rd AAAI Conf. Artif. Intell. AAAI 2019, 31st Innov. Appl. Artif. Intell. Conf. IAAI 2019 9th AAAI Symp. Educ. Adv. Artif. Intell. EAAI 2019*, pp. 9472–9477, 2019.
- [28] J. Dai, C. L. P. Chen, X. Y. Xu, and P. Hu, “Condition monitoring on complex machinery for predictive maintenance and process control,” *Conf. Proc. - IEEE Int. Conf. Syst. Man Cybern.*, pp. 3595–3600, 2008, doi: 10.1109/ICSMC.2008.4811856.
- [29] N. Lee, M. H. Azarian, and M. G. Pecht, “An Explainable Deep Learning-based Prognostic Model for Rotating Machinery,” *arXiv Prepr. arXiv2004.13608*, 2020.
- [30] R. Bogue, “Sensors for condition monitoring: A review of technologies and applications,” *Sens. Rev.*, vol. 33, no. 4, pp. 295–299, 2013, doi: 10.1108/SR-05-

2013-675.

- [31] L. Guo, N. Li, F. Jia, Y. Lei, and J. Lin, “A recurrent neural network based health indicator for remaining useful life prediction of bearings,” *Neurocomputing*, vol. 240, pp. 98–109, 2017, doi: 10.1016/j.neucom.2017.02.045.
- [32] T. Van Tung and B.-S. Yang, “Machine Fault Diagnosis and Prognosis: The State of The Art,” *Int. J. Fluid Mach. Syst.*, vol. 2, no. 1, pp. 61–71, 2009, doi: 10.5293/ijfms.2009.2.1.061.
- [33] H. Swapnarekha, H. S. Behera, J. Nayak, and B. Naik, “Role of intelligent computing in COVID-19 prognosis: A state-of-the-art review,” *Chaos, Solitons and Fractals*, vol. 138, p. 109947, 2020, doi: 10.1016/j.chaos.2020.109947.
- [34] V. Papastefanopoulos, P. Linardatos, and S. Kotsiantis, “COVID-19: A comparison of time series methods to forecast percentage of active cases per population,” *Appl. Sci.*, vol. 10, no. 11, pp. 1–15, 2020, doi: 10.3390/app10113880.
- [35] M. Fakhfakh, B. Bouaziz, F. Gargouri, and L. Chaari, “ProgNet: Covid-19 prognosis using recurrent and convolutional neural networks,” *medRxiv*, pp. 1–7, 2020, doi: 10.1101/2020.05.06.20092874.
- [36] S. Hochreiter and J. Schmidhuber, “Long Short-Term Memory,” *Neural Comput.*, vol. 9, no. 8, pp. 1735–1780, 1997, doi: 10.1162/neco.1997.9.8.1735.
- [37] A. Sherstinsky, “Fundamentals of Recurrent Neural Network (RNN) and Long Short-Term Memory (LSTM) network,” *Phys. D Nonlinear Phenom.*, vol. 404, p. 132306, 2020, doi: 10.1016/j.physd.2019.132306.
- [38] S. Hochreiter, “Long Short-Term Memory,” vol. 1780, pp. 1735–1780, 1997.
- [39] A. Abbasi, F. Nazari, and C. Nataraj, “Application of long short-term memory neural network to crack propagation prognostics,” *Proc. Annu. Conf. Progn. Heal. Manag. Soc. PHM*, vol. 2020-June, 2020, doi: 10.1109/ICPHM49022.2020.9187033.
- [40] T. Petković, L. Petrović, I. Marković, and I. Petrović, “Ensemble of LSTMs and feature selection for human action prediction,” pp. 1–12, 2021, [Online]. Available: <http://arxiv.org/abs/2101.05645>.
- [41] B. Bialke, “High fidelity mathematical modeling of reaction wheel performance,” 1998.

- [42] E. Sobhani-Tehrani and K. Khorasani, “Identification For Nonlinear Systems Using Hybrid Approach,” *Master’s Thesis*. pp. 12-13,15,18,37,92, 2008.
- [43] J. M. Hacker, J. Ying, and P. C. Lai, “Reaction Wheel Friction Telemetry Data Processing Methodology and On-Orbit Experience,” *J. Astronaut. Sci.* 2015 623, vol. 62, no. 3, pp. 254–269, Nov. 2015, doi: 10.1007/S40295-015-0076-7.
- [44] C. Ciandrini, M. Gallieri, A. Giantomassi, G. Ippoliti, and S. Longhi, “Fault detection and prognosis methods for a monitoring system of rotating electrical machines,” *IEEE Int. Symp. Ind. Electron.*, pp. 2085–2090, 2010, doi: 10.1109/ISIE.2010.5637762.
- [45] V. Nguyen, J. Seshadrinath, D. Wang, S. Nadarajan, and V. Vaiyapuri, “Model-Based Diagnosis and RUL Estimation of Induction Machines under Interturn Fault,” *IEEE Trans. Ind. Appl.*, vol. 53, no. 3, pp. 2690–2701, May 2017, doi: 10.1109/TIA.2017.2669195.
- [46] “Multivariate Time Series Analysis with LSTMs figure - All Codeless | KNIME.” <https://www.knime.com/blog/multivariate-time-series-analysis-lstm-codeless> (accessed Aug. 10, 2021).
- [47] “How to Use Timesteps in LSTM Networks for Time Series Forecasting.” <https://machinelearningmastery.com/use-timesteps-lstm-networks-time-series-forecasting/> (accessed Jul. 02, 2021).
- [48] “Multivariate Time Series Forecasting with LSTMs in Keras.” <https://machinelearningmastery.com/multivariate-time-series-forecasting-lstms-keras/> (accessed Jul. 02, 2021).
- [49] “Multivariate Time Series Forecasting with LSTMs in Keras - nttrungmt-wiki.” <https://sites.google.com/site/nttrungmtwiki/home/it/data-mining/time-series-analysis/multivariate-time-series-forecasting-with-lstms-in-keras> (accessed Jul. 02, 2021).
- [50] K. Greff, R. K. Srivastava, J. Koutnik, B. R. Steunebrink, and J. Schmidhuber, “LSTM: A Search Space Odyssey,” *IEEE Trans. Neural Networks Learn. Syst.*, vol. 28, no. 10, pp. 2222–2232, 2017, doi: 10.1109/TNNLS.2016.2582924.
- [51] “Understanding LSTM Networks -- colah’s blog.” <https://colah.github.io/posts/2015-08-Understanding-LSTMs/> (accessed Jun. 09,

2021).

- [52] “List of Probability and Statistics Symbols | Math Vault.”
<https://mathvault.ca/hub/higher-math/math-symbols/probability-statistics-symbols/>
(accessed Aug. 23, 2021).
- [53] “Understand the Impact of Learning Rate on Neural Network Performance.”
<https://machinelearningmastery.com/understand-the-dynamics-of-learning-rate-on-deep-learning-neural-networks/> (accessed Jul. 20, 2021).
- [54] A. Rahimi, K. D. Kumar, and H. Alighanbari, “Failure prognosis for satellite reaction wheels using Kalman filter and particle filter,” *J. Guid. Control. Dyn.*, vol. 43, no. 3, pp. 585–588, 2020, doi: 10.2514/1.G004616.
- [55] “Aocs Framework Project.” <https://www.pnp-software.com/AocsFramework/AocsBackground.html> (accessed Aug. 09, 2021).
- [56] W. Bialke, “A Discussion of Friction Anomaly Signatures in Response to Electrical Discharge in Ball Bearings,” *Aerosp. Mech. Symp.*, vol. 44, pp. 55–68, 2018.
- [57] “CubeSat Reaction Wheels Control System SatBus 4RW | NanoAvionics.”
<https://nanoavionics.com/cubesat-components/cubesat-reaction-wheels-control-system-satbus-4rw/> (accessed Aug. 10, 2021).
- [58] “Low-Frequency Band - an overview | ScienceDirect Topics.”
<https://www.sciencedirect.com/topics/engineering/low-frequency-band> (accessed Jul. 21, 2021).

APPENDICES

Appendix A: Copyright Permissions SMC-IEEE

8/9/2021

Rightslink® by Copyright Clearance Center



- Home
- Help
- Live Chat
- Sign in
- Create Account



Use of A Data-Driven Approach for Time Series Prediction in Fault Prognosis of Satellite Reaction Wheel

Conference Proceedings:
2020 IEEE International Conference on Systems, Man, and Cybernetics (SMC)

Author: [::Md::] [::Sraju::] [::Islam::]; Afshin Rahimi

Publisher: IEEE

Date: 11-14 Oct. 2020

Copyright © 2020, IEEE

Thesis / Dissertation Reuse

The IEEE does not require individuals working on a thesis to obtain a formal reuse license, however, you may print out this statement to be used as a permission grant:

Requirements to be followed when using any portion (e.g., figure, graph, table or textual material) of an IEEE copyrighted paper in a thesis:

- 1) In the case of textual material (e.g., using short quotes or referring to the work within these papers) users must give full credit to the original source (author, paper, publication) followed by the IEEE copyright line © 2011 IEEE.
- 2) In the case of illustrations or tabular material, we require that the copyright line © [Year of original publication] IEEE appear prominently with each reprinted figure and/or table.
- 3) If a substantial portion of the original paper is to be used, and if you are not the senior author, also obtain the senior author's approval.

Requirements to be followed when using an entire IEEE copyrighted paper in a thesis:

- 1) The following IEEE copyright/ credit notice should be placed prominently in the references: © [year of original publication] IEEE. Reprinted, with permission, from [author names, paper title, IEEE publication title, and month/year of publication]
- 2) Only the accepted version of an IEEE copyrighted paper can be used when posting the paper or your thesis online.
- 3) In placing the thesis on the author's university website, please display the following message in a prominent place on the website: In reference to IEEE copyrighted material which is used with permission in this thesis, the IEEE does not endorse any of [university/educational entity's name goes here]'s products or services. Internal or personal use of this material is permitted. If interested in reprinting/republishing IEEE copyrighted material for advertising or promotional purposes or for creating new collective works for resale or redistribution, please go to http://www.ieee.org/publications_standards/publications/rights/rights_link.html to learn how to obtain a License from RightsLink.

If applicable, University Microfilms and/or ProQuest Library, or the Archives of Canada may supply single copies of the dissertation.

BACK CLOSE WINDOW

Appendix B: Copyright Permissions PHM-IEEE

8/9/2021

Rightslink® by Copyright Clearance Center



Home Help Live Chat Sign in Create Account



Fault Prognosis of Satellite Reaction Wheels Using A Two-Step LSTM Network

Conference Proceedings:
2021 IEEE International Conference on Prognostics and Health Management (ICPHM)
Author: [::Md:] [::Sraju:] [::Islam:]; Afshin Rahimi
Publisher: IEEE
Date: 7-9 June 2021

Copyright © 2021, IEEE

Thesis / Dissertation Reuse

The IEEE does not require individuals working on a thesis to obtain a formal reuse license, however, you may print out this statement to be used as a permission grant:

Requirements to be followed when using any portion (e.g., figure, graph, table or textual material) of an IEEE copyrighted paper in a thesis:

- 1) In the case of textual material (e.g., using short quotes or referring to the work within these papers) users must give full credit to the original source (author, paper, publication) followed by the IEEE copyright line © 2011 IEEE
- 2) In the case of illustrations or tabular material, we require that the copyright line © [Year of original publication] IEEE appear prominently with each reprinted figure and/or table
- 3) If a substantial portion of the original paper is to be used, and if you are not the senior author, also obtain the senior author's approval.

Requirements to be followed when using an entire IEEE copyrighted paper in a thesis:

- 1) The following IEEE copyright/ credit notice should be placed prominently in the references: © [year of original publication] IEEE. Reprinted, with permission, from [author names, paper title, IEEE publication title, and month/year of publication]
- 2) Only the accepted version of an IEEE copyrighted paper can be used when posting the paper or your thesis online.
- 3) In placing the thesis on the author's university website, please display the following message in a prominent place on the website: In reference to IEEE copyrighted material which is used with permission in this thesis, the IEEE does not endorse any of [university/educational entity's name goes here]'s products or services. Internal or personal use of this material is permitted. If interested in reprinting/republishing IEEE copyrighted material for advertising or promotional purposes or for creating new collective works for resale or redistribution, please go to http://www.ieee.org/publications_standards/publications/rights/rights_link.html to learn how to obtain a License from RightsLink.

If applicable, University Microfilms and/or ProQuest Library, or the Archives of Canada may supply single copies of the dissertation.

BACK

CLOSE WINDOW

© 2021 Copyright - All Rights Reserved | Copyright Clearance Center, Inc. | Privacy statement | Terms and Conditions
Comments? We would like to hear from you. E-mail us at customer care@copyright.com

VITA AUCTORIS

NAME: Md Sirajul Islam

PLACE OF BIRTH: Narayanganj, Dhaka, Bangladesh

YEAR OF BIRTH: 1992

EDUCATION: Government Laboratory High School & College, Mirpur Rd,
Dhaka 1205, Bangladesh, 2010

Military Institute of Science and Technology, B.Sc., Dhaka 1216,
Bangladesh, 2015